Accepted Manuscript

Synthesis and evaluation of clioquinol-rolipram/roflumilast hybrids as multitarget-directed ligands for the treatment of Alzheimer's disease

Jinhui Hu, Tingting Pan, Baijiao An, Zhengcunxiao Li, Xingshu Li, Ling Huang

PII: S0223-5234(18)31050-X

DOI: https://doi.org/10.1016/j.ejmech.2018.12.013

Reference: EJMECH 10946

To appear in: *European Journal of Medicinal Chemistry*

Received Date: 16 October 2018

Revised Date: 4 December 2018

Accepted Date: 6 December 2018

Please cite this article as: J. Hu, T. Pan, B. An, Z. Li, X. Li, L. Huang, Synthesis and evaluation of clioquinol-rolipram/roflumilast hybrids as multitarget-directed ligands for the treatment of Alzheimer's disease, *European Journal of Medicinal Chemistry* (2019), doi: https://doi.org/10.1016/j.ejmech.2018.12.013.

Graphical Abstracts

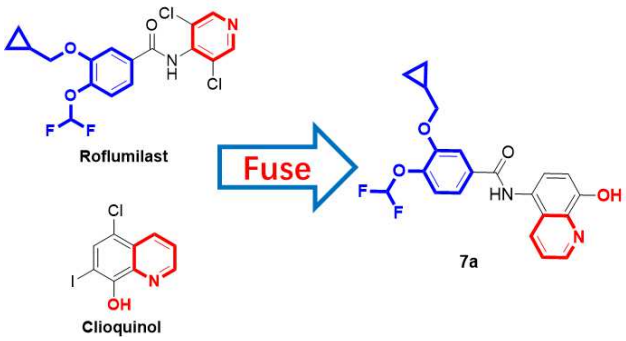

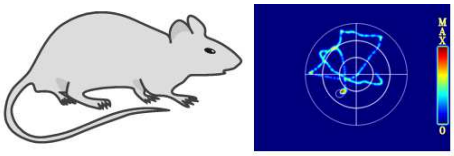

Inhibition of **PDE4D** (IC_{50} = 0.399 μM)

Modulation of metal-induced Aβ aggregation

Intracellular **antioxidant**

Ability of crossing **blood brain barrier** in vitro

Protection of hippocampal neurons from necrosis

Synthesis and evaluation of clioquinol-rolipram/roflumilast hybrids as multitarget-directed ligands for the treatment of Alzheimer's disease

Jinhui Hu, Tingting Pan, Baijiao An, Zhengcunxiao Li, Xingshu Li*, Ling Huang*

School of Pharmaceutical Sciences, Sun Yat-sen University, Guangzhou 510006, China

Abstract: Considering the importance of PDE4D inhibition and the modulation of biometals in Alzheimer's disease (AD) therapeutics, we have designed, synthesized and evaluated a series of new clioquinol-rolipram/roflumilast hybrids as multitarget-directed ligands for the treatment of AD. *In vitro* studies demonstrated that some of the molecules processed remarkable inhibitory activity against phosphodiesterase 4D (PDE4D), strong intracellular antioxidant capacity, potent inhibition of metal-induced aggregation of Aβ, and potential blood-brain barrier permeability. Compound **7a** demonstrated significant improvement in cognitive and spatial memory in an $A\beta_{25-35}$-induce mouse model in Morris water-maze test (MWM). These results indicate that compound **7a** is a promising multifunctional candidate that is worthy of further study.

Keywords: Alzheimer's disease, multitarget-directed ligands, PDE4D inhibitors, metal chelating agents.

Highlights:

New compounds with multifunctional activities against AD were synthesized and evaluated.

Compound **7a** exhibited effective PDE4D inhibitory potency, biometal chelating activities and BBB permeability.

Compound **7a** enhanced $A\beta_{25-35}$-induced cognitive and memory impairment in mice.

Introduction

Alzheimer's disease (AD), a progressive neurodegenerative disorder that is characterized by memory loss and a decline of language skills and recognition, occurs most frequently in elderly people. The World Alzheimer Report reported that there are 47 million people living with dementia, and the number would increase to more than 131 million by 2050 because of an aging population.[1]-[2] Due to the complexity of the pathogenesis, there is currently no drug that can completely treat AD. Among the many factors that cause AD, aberrant protein processing is a major pathological hallmark in which β-amyloid (Aβ) can form oligomers, fibrils and insoluble plaques.[3] Studies have confirmed that the levels of biometals including Cu^{2+}, Zn^{2+} and Fe^{2+} are redundant in the brains of AD patients (for copper, about 400 μM; for zinc and iron, about 1 mM),[4] which, along with β-amyloid peptides, are the main ingredients of these plaques.[5-7] Complexes of Aβ and metal ions can promote Aβ aggregation and trigger the generation of reactive oxygen species (ROS) which may initiate neuronal death and synaptic damage.[8-10] In addition, copper metabolism

proteins are related to AD.[11, 12] Therefore, as one approach for the treatment of AD, the regulation of biometal-Aβ interactions and amelioration the distribution of metals in the AD patients' brain seem to be a promising strategy. Studies have demonstrated that clioquinol (CQ) and its analogs can significantly improve cognition[13-15] and that these compounds can eliminate copper(II) from β-amyloid to prevent Aβ aggregates resulting in promoting degradation of extracellular Aβ peptides.[16, 17] The multitarget-directed metal-chelating agents HLA-20A and IQM-622 have been developed.[18, 19]

Neuroinflammation is closely associated with the pathogenesis of AD.[20] Phosphodiesterase 4 (PDE4) belongs to the phosphodiesterase subfamily of enzymes that can hydrolyze the intracellular second messenger cAMP.[21] PDE4D is a subtype of PDE4s (PDE4A to PDE4D) that has relatively high expression in the frontal cortex.[22] PDE4D is one of the key subtypes participating in the process of memory consolidation and long-term potentiation (LTP),[23] and PDE4B is involved in neuroinflammation.[24] Recently, several strategies have been proposed to enhance the levels of cerebral cyclic adenosine monophosphate (cAMP) for the treatment of neurodegenerative diseases by the inhibition of PDEs.[25-28] The PDE4 inhibitor rolipram not only facilitates memory performance in both LTP and contextual learning but also repairs spine density to normal levels in APP/PS1 transgenic mouse model of AD.[29] A preclinical research demonstrated that roflumilast (another PDE4 inhibitor) could improve cognitive deficits in rodent behavior experiments such as new object recognition tasks and the Y-maze test. Currently, one Phase II study of the

enhancement of translational cognition by roflumilast, and one Phase I study have been completed which was to evaluate the co-administration of roflumilast and donepezil for ameliorating scopolamine-induced cognitive performance.[30, 31] The newly developed PDE4D, GEBR-32a, can enhance spatial and object recognition performance in AD transgenic mice (Figure 1).[28, 32]

Due to the complicated pathogenesis and progression of neurodegenerative diseases, the development of multitarget-directed ligands (MTDLs) that possess two or more complementary biological activities for the treatment of AD, has been of interest in recent years.[15, 33-35] Taking into account the importance of PDE4D inhibition and the modulation of biometals in AD therapeutics,[36] we fused the key binding site fragments of rolipram/roflumilast and linking it to the metal ion chelator framework of CQ to obtain a series of hybrids. Herein, we report on the design, synthesis and evaluation of PDE4D inhibitory activity, the inhibition of Cu^{2+}-induced Aβ aggregation, potential blood-brain barrier (BBB) penetration, antioxidation, and an assessment of the water maze model for AD.

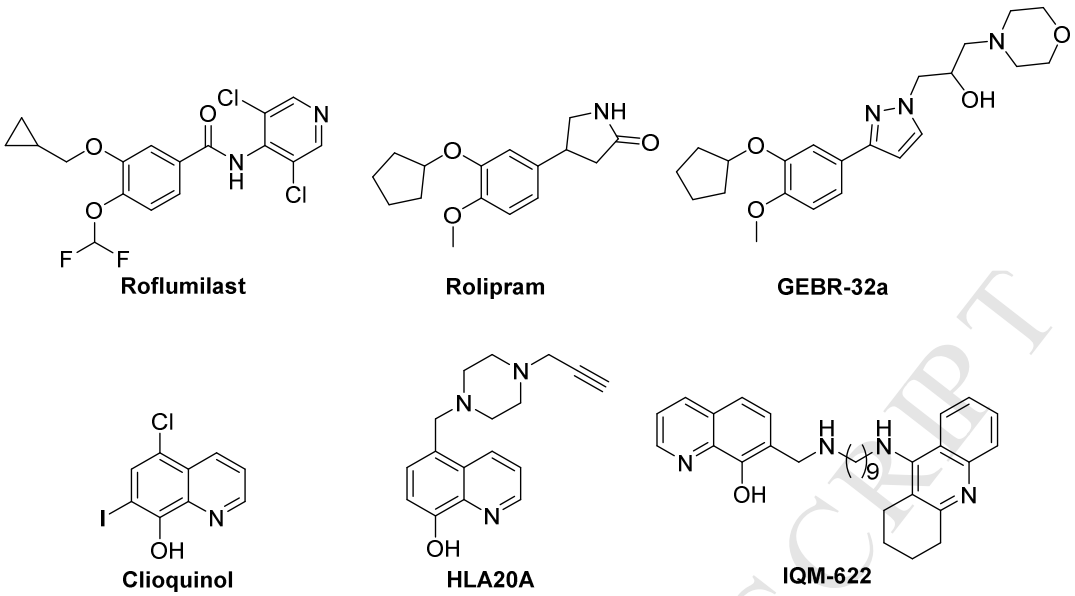

Figure 1. Structures of PDE4D inhibitors and multitarget-directed metal-chelating agents.

Results and discussion

Chemistry. We have synthesized eight hybrids (**5a-b**, **6a-c**, **7a-c**) by coupling the fragment of PDE4 inhibitors roflumilast and rolipram at the 5-position of 8-hydroxyquinoline. Their synthetic routes are described in Scheme 1. Intermediates **1a-c** were prepared in accordance with a literature procedure.[37] The reaction of amines **1a-c** with corresponding substituted benzoyl chlorides yielded amides **2a-b**, **3a-c** and **4a-c**. Deprotection of the t-butyloxy carbonyl group with hydrogen chloride produced compounds **5a-b**, **6a-c** and **7a-c**.

Scheme 1. Synthesis of Compounds **5a-b**, **6a-c**, **7a–c**[a]

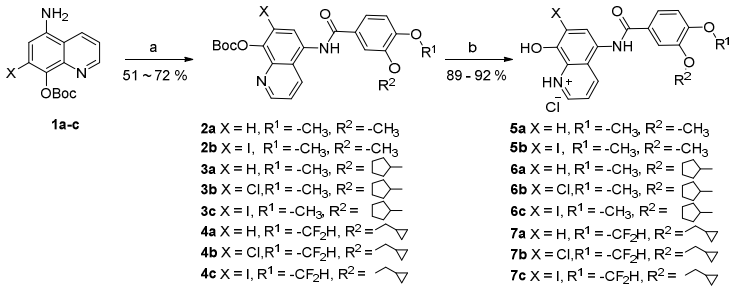

[a] Reagents and conditions: (a) i). benzoic acid, $SOCl_2$, reflux; ii) anhydrous CH_2Cl_2, TEA, room

temperature; (b) CH_2Cl_2:CH_3OH = 5:1, HCl (gas).

The preparation of compounds **13a-b** and **14a-b** is summarized in Scheme 2. The starting materials 2-methylquinolin-8-ol **8a** and 5,7-dichloro-2-methylquinolin-8-ol **8b** were reacted with benzyl chloride, and the subsequent oxidation of the methyl group by SeO_2 provided aldehydes. By the Pinnick oxidation, aldehydes were easily converted to carboxylic acids **10a** and **10b**. By reaction with $SOCl_2$, and then with corresponding amine analogues, **10a** and **10b** were converted to **11a-b** and **12a-b**, which provided the target compounds **13a-b** and **14a-b** by removal of the Bn group under an H_2 atmosphere.

Scheme 2. Synthesis of Compounds **13a-b** and **14a-b** [a]

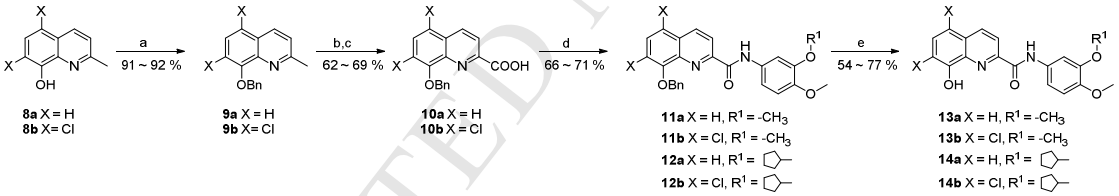

[a] Reagents and conditions: (a) benzyl bromide, K_2CO_3, acetone; (b) SeO_2,1,4-dioxane; (c) $NaClO_2$, NaH_2PO_4, CH_3CN/H_2O; (d) i) $SOCl_2$; ii) 3-(cyclopentyloxy)-4-methoxyaniline or 3,4-dimethoxyaniline, anhydrous CH_2Cl_2, TEA, room temperature; (e) H_2, Pd / C, CH_3OH.

Scheme 3 shows the synthesis of target compounds **18a-b**. Quinolin-8-ol **15** was converted to TBS-protected 2-aminoquinolin-8-ol **16** by using previous reported methods.[38] Compound **16** was treated with the corresponding benzoyl chlorides to provide compounds **17a-b**. Finally, deprotection of **17a-b** afforded target compounds **18a-b.**

Scheme 3 Synthesis of Compounds **18a-b**[a]

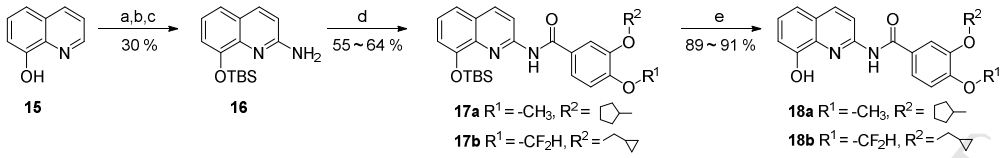

[a]Reagents and conditions: (a) mCPBA, CH_2Cl_2; (b) i) $(CH_3O)_2SO_2$, CH_3CN; ii) $NH_3 \cdot H_2O$; (c) TBSCl, DIPEA, THF; (d) substituent acyl chloride, DIPEA, THF; (e) TBAF, THF.

Biology. PDE4D inhibitory activity. Considering that PDE4D is one of the key subtypes participating in LTP, we chose PDE4D for screening with rolipram as the reference compound to evaluate the PDE4D inhibitory activities of the synthesized hybrids by using a previously described method.[39] As the results show in Table 1, **6a-c** and **7a-c**, possessing 3-cyclopentyloxy-4-methoxy and 3-cyclopropylmethoxy-4-difluoromethoxy groups at the benzamide moiety, exhibited potent inhibitory activities with IC_{50} values ranging from 0.399 to 3.83 μM, in contrast to their analogues **5a** and **5b** (IC_{50}: 7.63 and 7.36 μM) which possess two methoxy groups at the same position. Further examination of the relationship between structure and activity indicated that substituents at the 7-position of the 8-hydroxyquinoline moiety also have a great influence on the activity. Compounds **6a**, **6c**, **7a** and **7c**, possessing hydrogen or iodine at the 7-position, provided much better activities (IC_{50}: 0.492, 0.597, 0.399 and 0.426 μM for **6a**, **6c**, **7a** and **7c**) than did chlorine at the same position (IC_{50}: 3.13 and 3.83 μM for **6b** and **6b**), which might be related to the poor solubility of **6b** and **6b** in the buffer. Compounds **14a-b** and **18a-b**, in which 3-(cyclopentyloxy)-4-methoxybenzamide or

3-cyclopropylmethoxy-4-difluoromethoxy benzamide moieties are joined at the 2-position of 8-hydroxyquinoline, also provided moderate PDE4D inhibitory activities with IC_{50} values ranging from 4.06 to 6.78 μM, suggesting that coupling pharmacophores at this position might be not beneficial. Comparing the activities of **13a** and **14b**, we conclude that chlorine at the 5- and 7-positions of 8-hydroxyquinoline moiety was unfavorable.

Table 1. PDE4D inhibitory activity, oxygen radical absorbance capacity (ORAC value), *P*e value from the PAMPA-BBB assay for selected compounds and prediction of potential penetration into the CNS [a]

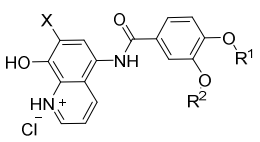

5a-c, 6a-c, 7a-c

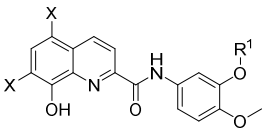

13a-b,14a-b

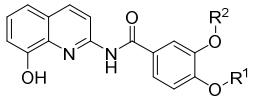

18a-b

Comd.	X	R^1	R^2	PDE4D2 IC_{50} (μM) [a]	ORAC [b]	*Pe* ($\times 10^{-6}$ cm s^{-1}) [c]	Pred.
5a	H	CH_3	CH_3	7.63 ± 0.21	1.34 ± 0.17	NT	NT
5b	I	CH_3	CH_3	7.36 ± 0.28	1.30 ± 0.045	NT	NT
6a	H	CH_3		0.492 ± 0.007	0.63 ± 0.069	5.90 ± 0.31	CNS+
6b	Cl	CH_3		3.13 ± 0.11	0.56 ± 0.021	NT	NT
6c	I	CH_3		0.597 ± 0.024	1.01 ± 0.030	5.86 ± 0.70	CNS+
7a	H	CF_2H		0.399 ± 0.021	0.60 ± 0.013	12.92 ± 0.82	CNS+
7b	Cl	CF_2H		3.83 ± 0.14	0.74 ± 0.065	NT	NT
7c	I	CF_2H		0.426 ± 0.067	0.69 ± 0.023	7.05 ± 0.96	CNS+
13a	H	CH_3	-	4.32 ± 0.15	1.03 ± 0.039	NT	NT
13b	Cl	CH_3	-	8.07 ± 0.26	1.05 ± 0.058	NT	NT
14a	H		-	4.15 ± 0.19	1.98 ± 0.093	NT	NT
14b	Cl		-	6.78 ± 0.27	1.29 ± 0.011	NT	NT
18a	-	CH_3		4.64 ± 0.17	0.70 ± 0.050	16.41 ± 0.44	CNS+
18b	-	CF_2H		4.06 ± 0.32	0.34 ± 0.045	15.77 ± 0.42	CNS+
Rolipram				0.621 ± 0.028	0.070 ± 0.010	18.87 ± 0.57	CNS+
Roflumilast				0.480 ± 0.035	0.067 ± 0.015	9.22 ± 0.62	CNS+
CQ				>10	0.60 ± 0.047	5.20 ± 0.33	CNS+

[a] Values are expressed as mean ± SD from triplicate independent experiments. [b] ORAC values are expressed as trolox equivalents. [c] *Pe* Values are expressed as the mean ± SD from at least triplicate independent experiments. Compounds could potential cross the BBB when $Pe > 4.7 \times 10^{-6}$ cm s^{-1}. NT = not test.

Free oxygen radical absorbance capacity. Oxidative stress is an important event in the pathogenesis and progression of AD.[40] To evaluate the antioxidant activity of these compounds, we performed the free oxygen radical absorbance capacity (ORAC) assay with the vitamin E analogue Trolox as the reference. Compounds **6a-c** and **7a-c**, which possess 3-cyclopentyloxy-4-methoxy or 3-cyclopropylmethoxy-4-difluoromethoxy in the benzamide moiety, exhibited nearly the same ORAC values as that of clioquinol (0.60 ± 0.047 ORAC value). In comparison with the target compounds, rolipram and roflumilast provided very weak antioxidative abilities, with ORAC values of 0.070 and 0.067, respectively. It appears that the 3,4-dimethoxybenzamide moiety was slightly favorable for providing antioxidant activity. Compound **5a-b** and **13a-b** produced ORAC values of 1.03-1.34, better than those of **6a-c** and **7a-c**.

***In vitro* blood–brain barrier penetration assay**. Whether or not CNS drugs could be effective, one important issue is if they can pass through the blood-brain barrier (BBB). We have performed the parallel artificial membrane permeation assay (PAMPA) to evaluate the potential BBB permeability of the selected compounds. [41] By comparing the permeability of thirteen commercial drugs with reported values to validate the assay, a plot of experimental permeability (*Pe*) versus reported values was constructed using this assay and produced a linear correlation of *Pe* (exp.) = 1.4574*Pe* (lit.) - 1.0773 (R^2 = 0.9427). From this equation, and considering the limit established in the literature, *Pe* value of compounds was greater than 4.7×10^6 cm·s^{-1} indicating that the compound has potential BBB permeability. As the results in Table 1

demonstrate, all the tested compounds with a *Pe* value greater than 4.7×10^6 cm·s^{-1} could potentially cross the BBB (**6a**, 5.90 ± 0.31; **6c**, 5.86 ± 0.70; **7a**, 12.92 ± 0.82; **7c**, 7.05 ± 0.96; **18a**, 16.41 ± 0.44; **18b**, 15.77 ± 0.42). The *Pe* values for rolipram, roflumilast and CQ were determined to be 18.87 ± 0.57, 9.22 ± 0.62 and 5.20 ± 0.33, respectively.

Metal-chelating properties of compounds 6a and 7a. After consideration of their PDE4D inhibitory activity, antioxidant activity and ability to pass the BBB, compounds **6a** and **7a** were selected for further study with CQ as a reference. An ultraviolet–visible spectroscopy assay was performed to determine their ability to chelate biometals including Cu^{2+}, Fe^{2+}, Fe^{3+} and Zn^{2+}. As shown in Figure 2 (A, B and C), compound **6a** exhibits a maximum absorption at 243 nm with a secondary peak at 223 nm in HEPES buffer. When $CuSO_4$ was added into the solution, the maximum absorption shifted to 267 nm, indicating the formation of a **6a**-Cu(II) complex. Likewise, a maximum absorption at 263 nm for **6a** + Zn^{2+} also indicates the coordination of compound **6a** with this metal. Compound **7a** in buffer exhibited a maximum absorption at 243 nm and a secondary peak was at 223 nm. New absorbance bands were at 285 nm and 277 nm when $CuSO_4$ and $ZnCl_2$ were added into the solution of **7a**. Even though there was no obvious absorbance change with the addition of $FeSO_4$ or $FeCl_3$ to the solution of **6a** and **7a**, the disappearance of the secondary peak indicated that there was potential interaction between the Fe^{2+}, Fe^{3+} and the compounds. To confirm the components of the complex, the binding stoichiometry of **6a** and **7a** with Cu^{2+} was determined by measuring the changes in

absorption at 415 and 422 nm, respectively. As shown in Figure 2D and 2E, the results of titration analysis indicated that the Cu^{2+} / ligand molar ratio is 1 : 2, which is consistent with the added amount of $CuSO_4$ and compound **6a** or **7a**. These results are in accordance with that of CQ (Figure 3F).

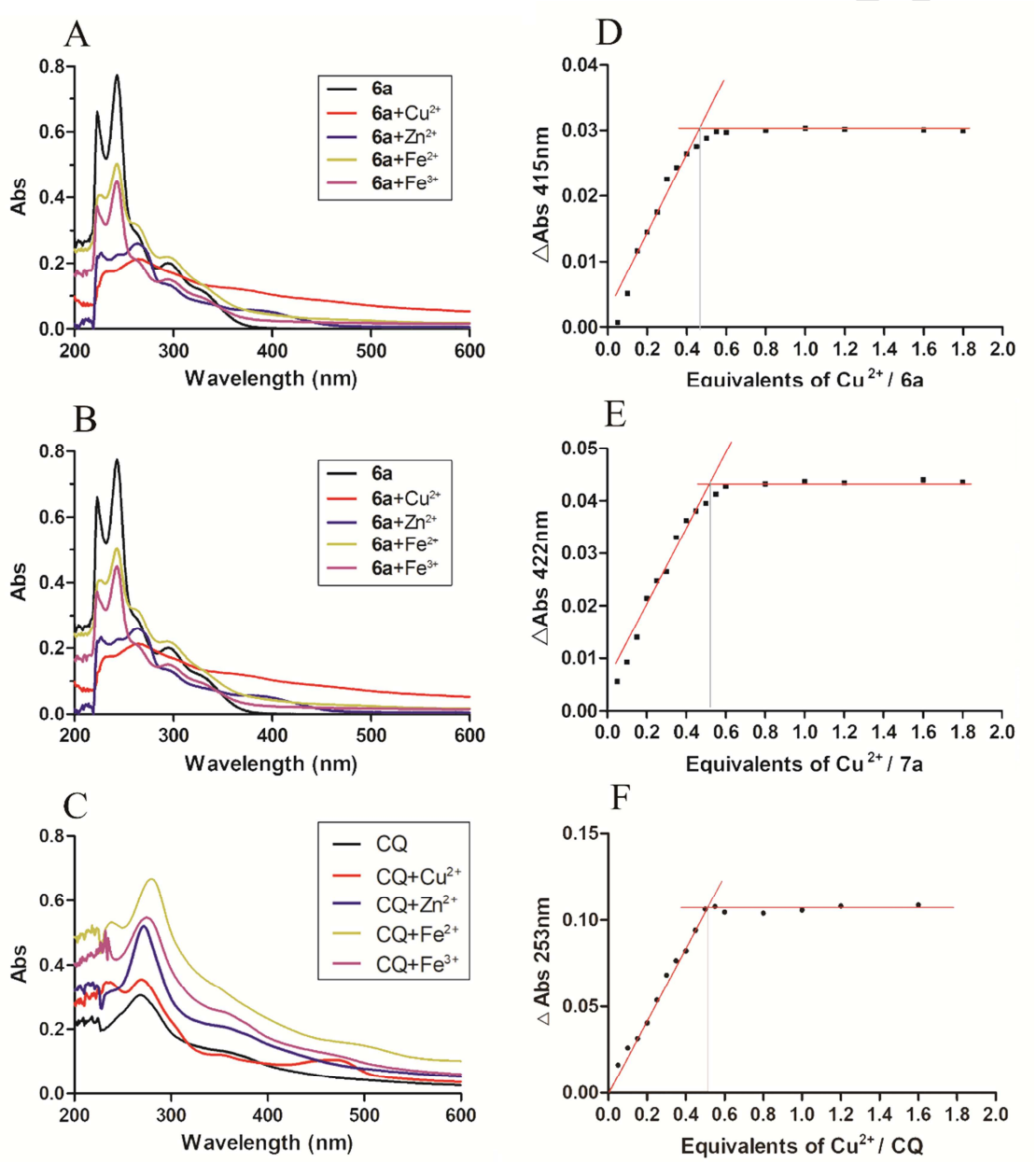

Figure 2. (A, B and C) UV-vis absorption spectra of compounds **6a**, **7a** and CQ (50 μM) with Cu^{2+}, Zn^{2+}, Fe^{2+} or Fe^{3+}(50 μM) in HEPES buffer. (D, E and F) UV-vis titration of **6a, 7a** and CQ in the present of Cu^{2+} in HEPS buffer. The concentrations of Cu^{2+} and **6a**/**7a**/CQ were 0-144 μM

and 80 μM, respectively. Breakpoints are observed at [Cu^{2+}] : [**6a**/**7a**/CQ] = 0.5 : 1.

Inhibition of ROS produced in the Cu^{2+}-ascorbate system. Reactive oxygen species (ROS) play a key role in the pathogenesis of AD, and accumulated evidence suggests that the production of ROS is dependent on the redox of metal ions. Redox-active metal ions, especially redox-active Cu^{2+}, can catalyze the generation of ROS which triggers neuronal cell death in AD patients. To evaluate the ability of metal chelators **6a** and **7a** to prevent copper redox cycling under aerobic conditions, the copper redox cycling model was used as described by Faller and coworkers (Figure 3A).[42] Hydroxyl radicals (OH·) were generated by Cu-ascorbate redox system with ascorbate and were determined by their reaction with coumarin-3-carboxylic acid (CCA) to generate fluorescent 7-hydroxy-coumarin-3-carboxylic acid. The fluorescence of the copper-ascorbate system increased linearly with time for approximately 400 s and reached a plateau at about 700 s, demonstrating a marked production of OH· (Figure 3B). In contrast, there was no significant production of HO· when **6a** and **7a** were co-incubated with the Cu(II)-ascorbate system, suggesting these compounds could prevent the copper redox cycling by metal chelation. The metal chelator CQ was used as a control.

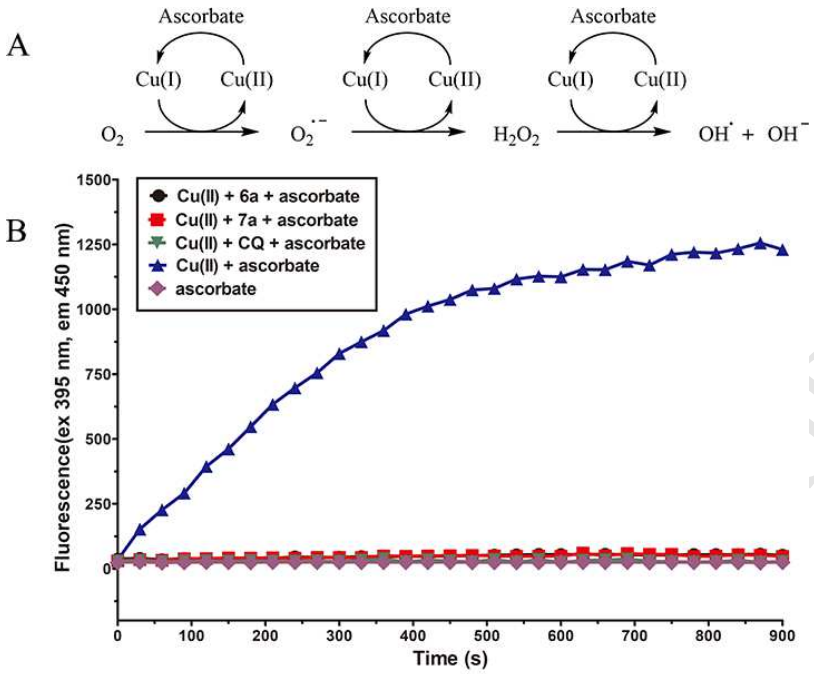

Figure 3. (A) Production of hydroxyl radicals in the copper-ascorbate system (B) Fluorescence intensity of copper-ascorbate-**6a**, copper-ascorbate-**7a**, copper-ascorbate-CQ, copper-ascorbate and ascorbate alone systems (excitation: 395 nm; emission: 450 nm). Coumarin-3-carboxylic acid (50 μM), ascorbate (150 μM), Cu(II) = 5 μM, **6a**, **7a** and CQ =10 μM. PBS (pH = 7.4), 37 °C.

Intracellular antioxidant assay. To evaluate the *in vivo* antioxidant activity of **6a-b** and **7a-b**, an intracellular antioxidant assay was determined using 2',7'-dichlorofluorescein diacetate (DCFH-DA) in SH-SY5Y cells. First, the cytotoxicity of the compounds was evaluated using an MTT assay by assessing the viability of SH-SY5Y cells. The results are summarized in Figure 4A. Compounds **6a** and **7a** showed no effect on the cell viability at a concentration of 10 μM, while **6b** and **7b** exhibited some cytotoxic effect at this concentration. Therefore, we chose **6a** and **7a** for use in the cellular antioxidant assay. The ROS level was remarkably increased when treating with t-BuOOH on SH-SY5Y cells (Figure 4B). Compound **7a** exhibited a concentration-dependent protective effect against t-BuOOH-induced intracellular

oxidative stress, which suggested that **7a** may be an efficient multifunctional agent for further study.

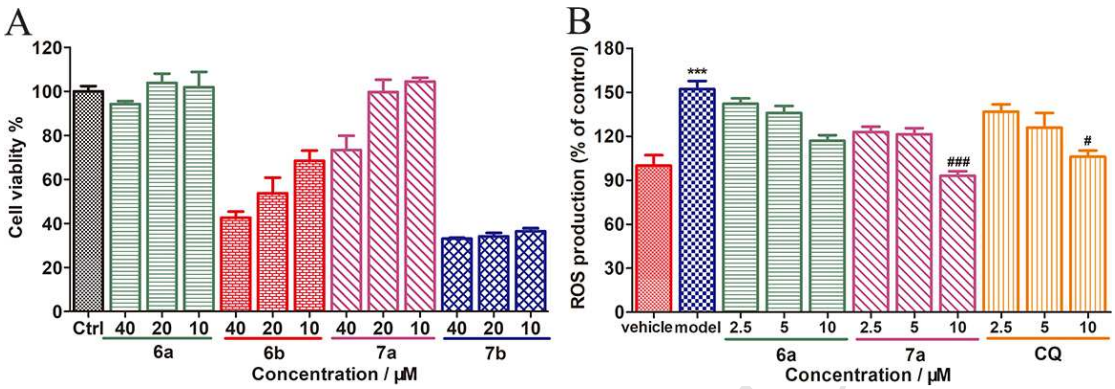

Figure 4. (A) Cell viability of **6a-b** and **7a-b** on SH-SY5Y cells. (B) t-BuOOH-induced ROS without or with the treatment of compounds by using DCFH-DA. The results are expressed as the percent of vehicle control in three independent experiments. ***, $p < 0.001$ vs the vehicle group; #, $p < 0.05$, ###, $p < 0.001$ vs the model group.

Inhibition of metal-induced Aβ aggregation. High levels of biometals (copper and zinc) in AD patients may potentially be the cause of neurotoxicity. We have performed the thioflavin T (ThT) fluorescence assay to evaluate the inhibitory activity of the target compounds against metal-induced Aβ aggregation with clioquinol (CQ) as a positive control. The fluorescence units increased from 100 % (Aβ alone) to 156 % (Aβ + Cu(II)) after the addition of $CuSO_4$ (Figure 5A). The fluorescence units were decreased significantly when CQ and compounds **6a**, **6b**, **7a** and **7b** were incubated with Aβ and Cu(II). The results indicated that these compounds can strongly prevent Cu(II)-induced Aβ aggregation. Furthermore, compounds **6a** and **7a** were more potent than CQ (Aβ + Cu(II) + CQ, 66 %; Aβ + Cu(II) + **6a**, 46 %; Aβ + Cu^{2+} + **6a**, 51 %).

While **6b** and **7b** were slightly less potent than CQ (Aβ + Cu^{2+} + **6b**, 70.2 %; Aβ + Cu^{2+} + **7b**, 82 %). Based on the ThT assay, morphological changes in the Aβ species were studied by transmission electron microscopy (TEM). A marked production of Aβ fibrils was detected in Cu(II)-treated samples of fresh Aβ (Figure 5B, sequence 2). In contrast, smaller and amorphous conformations of Aβ aggregates were observed when compounds **6a**, **7a** and CQ were incubated with Cu(II)-treated Aβ samples (Figure 5B, sequences 3, 4 and 5), which was consistent with results of the ThT fluorescence assay. Overall, ThT and TEM assay results jointly demonstrated that compounds **6a** and **7a** have the potential inhibit metal-induced $Aβ_{1-42}$ aggregation.

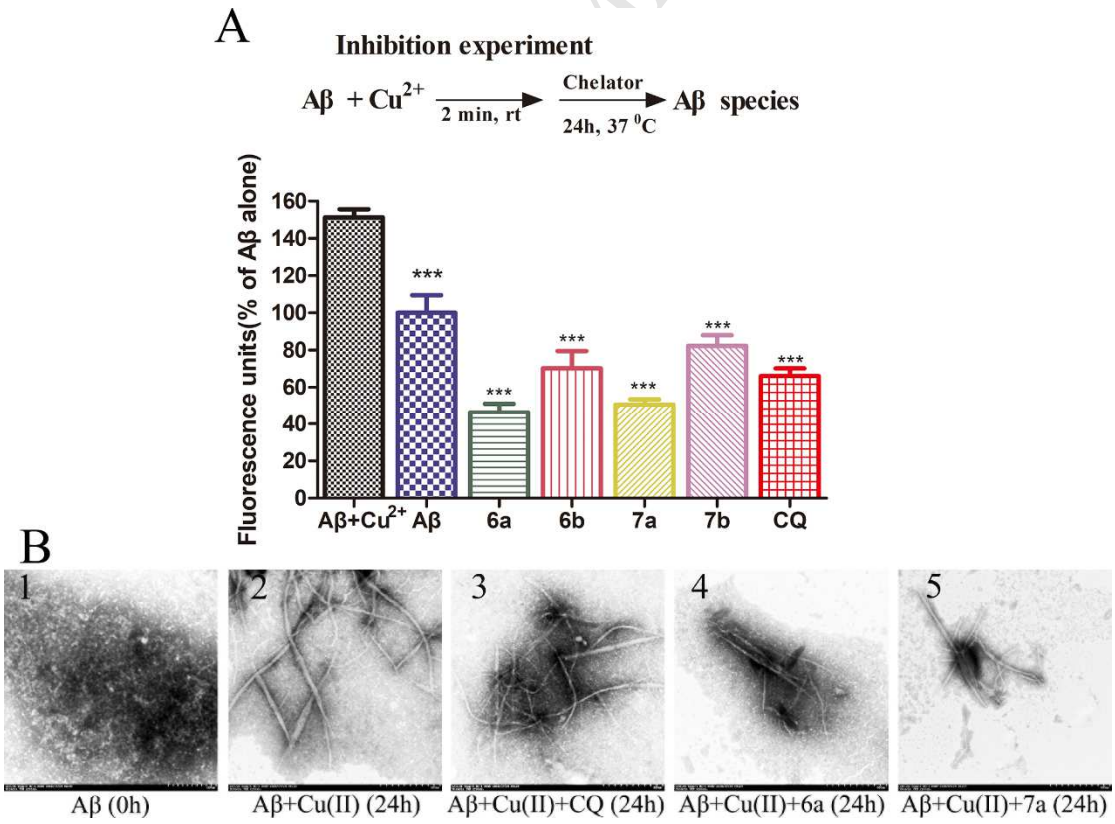

Figure 5. Inhibition by test compounds of Cu^{2+}-induced $Aβ_{1-42}$ aggregation (A) Top: Scheme of the inhibition experiment. Bottom: Results of the thioflavin T fluorescence binding assay. Data are

expressed as the mean ± SD in three independent experiments. *** $p < 0.001$, versus the Aβ + Cu(II) group. (B) Visualization by TEM of the inhibition by compounds **6a** and **7a** on Cu^{2+}-induced $A\beta_{1-42}$ aggregation.

Molecular docking studies. Molecular docking studies were performed to investigate the potential binding sites of compounds **6a** and **7a** with PDE4D. The molecular docking results of the PDE4 crystal structure (PDB code: 1XOQ) with compounds **6a** and **7a** are shown in Figure 6 with roflumilast as a reference. Compounds **6a** and **7a** were both sandwiched by the hydrophobic residues Phe372 and Ile336. Cyclopentyl and methyl oxygen of **6a**, and cyclopropylmethyl and difluoromethyl oxygen of **7a** formed hydrogen-bonds with the amide nitrogen of the Gln369 side chain (Figures 6A and 6B). The hydrogen bond between Gln369 and stacking on Phe372 of roflumilast (ROF) are shown in Figure 6C. It deserves mention that the binding mode of **7a** was very similar to that of roflumilast (Figure 6D), which may explain the relatively better activity in the enzyme.

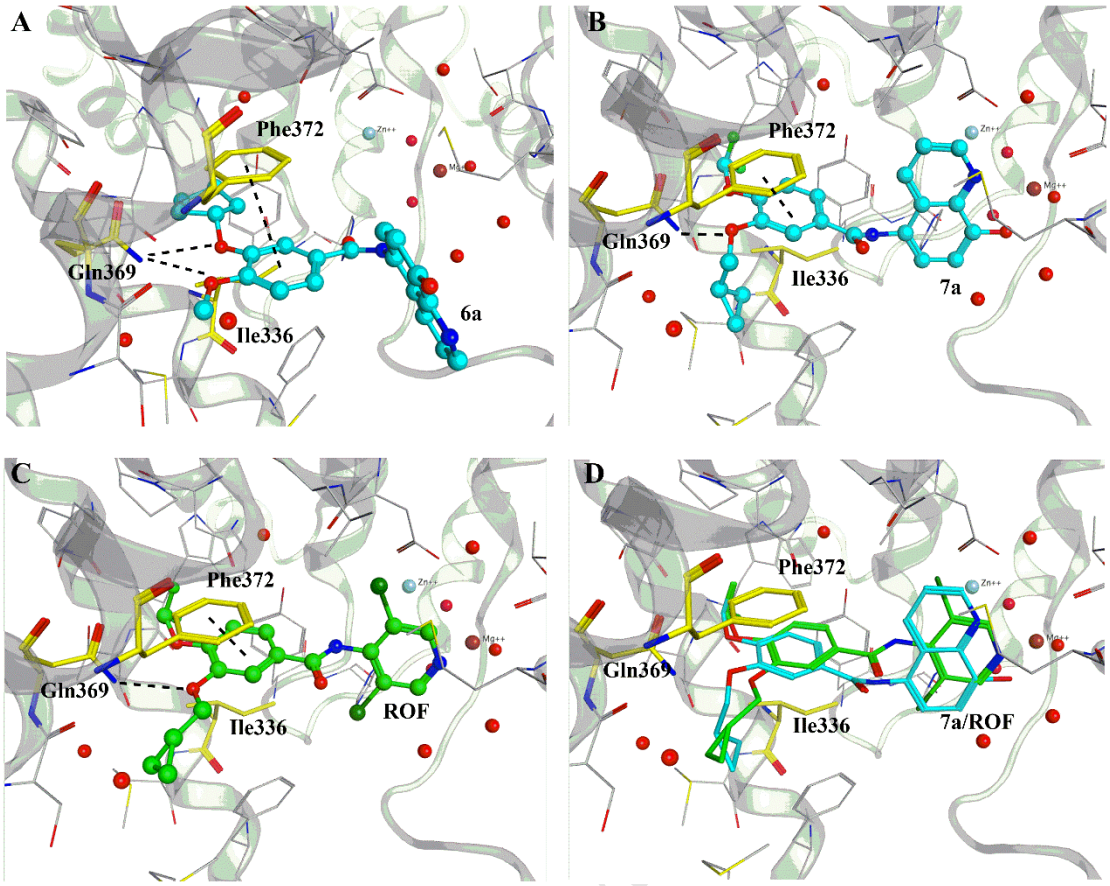

Figure 6. Compounds **6a** and **7a** in the PDE4D (PDB: 1XOQ) binding sites with roflumilast (ROF). (A) Binding mode for **6a** (shown in cyan); (B) Binding mode for **7a** (shown in cyan); (C) Binding mode for roflumilast (ROF) (shown in green); (D) Comparison of the binding modes for compounds **7a** and roflumilast (ROF) (**7a** is colored in cyan and roflumilast is colored in green). The backbone of PDE4D is shown as a ribbon representation. The dashed lines show hydrogen-bonds as well as stacking between Phe372 and the aromatic ring of the inhibitors.

Acute toxicity of compounds 6a and 7a. To investigate the safety properties of compounds **6a** and **7a**, acute toxicity experiments were performed. After intragastric administration of compounds **6a** and **7a** with various dosages, none of the mice died or were found to exhibit any abnormal behavior over the following 14 days.[43] The organs (heart, liver, lungs and kidneys) of mice were examined after sacrifice on the 14th day . No apparent abnormal changes and damages in their organs were found in

both compounds **6a** and **7a** groups. In general, compounds **6a** and **7a** exhibited safety and well tolerated up to 2000 mg/kg which can use for further *in vivo* study.

Metabolic stability of compounds 6a and 7a. To assess drug-like properties of compound 6a and 7a, the metabolic stability assay was performed by using rat liver microsomes with CQ and donepezil as standards and testosterone as a positive control. Compounds **6a** and **7a** exhibited $T_{1/2}$ values of 51.7 and 90.3 min, respectively, in liver microsomes (Table 2). The half-lives of testosterone ($T_{1/2}$ = 2.3 min), donepezil ($T_{1/2}$ = 75.6 min) and CQ ($T_{1/2}$ = 35.8 min) were consistent with previous reports.[44, 45] These results suggested that compound **6a** and **7a** were potentially metabolic stable which could be carried out further studies *in vivo*.

Table 2. Metabolic stability of **6a** and **7a** in rat liver microsomes.

Compd	K (min^{-1})	$T_{1/2}$ (min)[a]
Testosterone	0.301 ± 0.033	2.3 ± 0.3
Donepezil	0.00917 ± 0.00044	75.6 ± 4.4
CQ	0.0194 ± 0.0013	35.8 ± 2.9
6a	0.0134 ± 0.0080	51.7 ± 3.3
7a	0.00767 ± 0.00040	90.3 ± 5.7

[a] Results are expressed as the mean ± SD from three independent experiments.

Cognitive and memory strengthening in a mouse model by oral uptake of 6a and 7a. To investigate the *in vivo* effects of candidate **6a** and **7a**, the Morris water-maze

test was performed on a $A\beta_{25-35}$-induced cognitive dysfunction in mice with rolipram, roflumilast and CQ as positive controls. Mice were randomly allocated into 7 groups: sham, model, rolipram, CQ, roflumilast, **6a** and **7a** groups.[46, 47] The mice in each group (except the sham group) received intracerebroventricular injections (ICV) of a solution of $A\beta_{25-35}$ (3 nmol). For the sham group, mice were received ICV with saline as the same volume. Then, the mice from each group were treated with corresponding drug dosages by intragastric administration for 26 consecutive days (the sham and model groups: 0.5 % CMC-Na solution; the rolipram group: 4 mg/kg; the roflumilast group: 4 mg/kg; the CQ group: 30 mg/kg; the **6a** group: 30 mg/kg, and the **7a** group: 30 mg/kg). As shown in Figure 7A, there was no significant loss of body weight or adverse or abnormal events (diarrhea, emesis-like behavior) during the drug administration period, indicating that compounds **6a** and **7a** were safe in mice at a dose of 30 mg/kg/day.

Twenty-one days later, training trials were performed by using the Morris water maze (MWM) task. The model group exhibited a longer escape latency and required more paths to find the hidden platform in the water pool compared to sham group. Compared with the model group, compounds **6a** and **7a** could reduce the escape latency and path for searching the platform. Escape latency for compound **7a** was shorter than that for rolipram, roflumilast and CQ, indicating that **7a** could strengthen the memory capability and cognitive functions in $A\beta_{25-35}$-induced AD mice (Figure 7B and 7C).

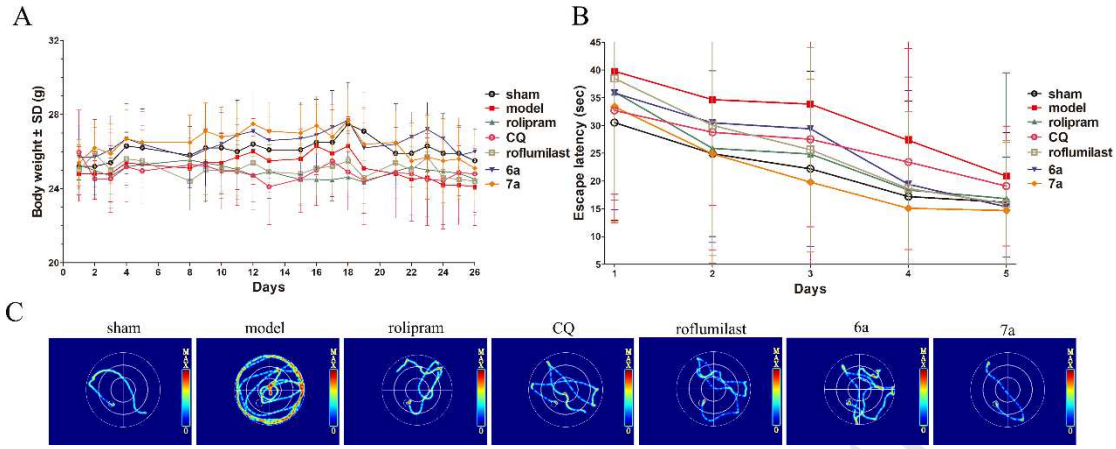

Figure 7. (A) Daily weight for each group (sham, model, rolipram, CQ, roflumilast, **6a** and **7a** groups) for 26 consecutive days (n = 11). (B) The escape latency for each group in training trials (mean ± SD, n = 11). (C) The representative tracks for each group in training trials.

A spatial probe trial in the MWM test was performed by removal of the platform after the training trials. The original platform location in the training trials was set as the virtual platform, and its 2-fold diameter area was set as the effective region. The number of virtual platform crossings, times in the effective region, as well as the paths in the virtual platform were recorded as neurobehavioral parameters. The results demonstrate that **6a** and **7a** provided approximately equivalent swimming speeds relative to the sham group, indicating that administration of compounds **6a** and **7a** have no effect on the motility and exploratory activities of the mice (Figure 8A, sham = 17.5 ± 2.3, model = 15.6 ± 2.4, rolipram = 15.1 ± 3.8, CQ = 16.0 ± 2.2, roflumilast = 14.5 ± 2.2, **6a** = 15.3 ± 2.1 and **7a** = 15.0 ± 2.8). The number of crossing the virtual platform in the model group (1.5 ± 1.3) was remarkably ($p < 0.01$) less than that of the sham group (3.63 ± 1.6), indicating that intrahippocampal injections of $A\beta_{25\text{-}35}$ lead to spatial learning and memory deficiency in mice (Figure 8B). The numbers of virtual

platforms in the roflumilast (3.8 ± 1.5, $p < 0.01$), **6a** (3.4 ± 1.7, $p < 0.05$) and **7a** (4.3 ± 1.9, $p < 0.001$) treatment groups were significantly increased compared with that of the model group. Furthermore, paths in the virtual platform and times in the effective region for the **6a** and **7a** groups (18.0 ± 7.0, $p < 0.05$ and 19.0 ± 8.0, $p < 0.5$; 6.1 ± 2.37 and 6.8 ± 2.2, $p < 0.1$) were remarkably longer than that for the model group (10.2 ± 3.2; 4.3 ± 1.3), indicating that compounds **6a** and **7a** could alleviate the deficits of learning and memory in mice induced by $A\beta_{25-35}$ with rolipram (16.5 ± 9.3; 5.7 ± 2.5), roflumilast (16.0 ± 9.0; 5.4 ± 1.6) and CQ (18.0 ± 12.7, $p < 0.5$; 5.8 ± 1.8) at the tested dosage (Figures 8C and D). Taken together, these results demonstrate that compound **7a** could significantly improve spatial learning and cognition functions. Compound **7a** is the most promising potential candidate against AD.

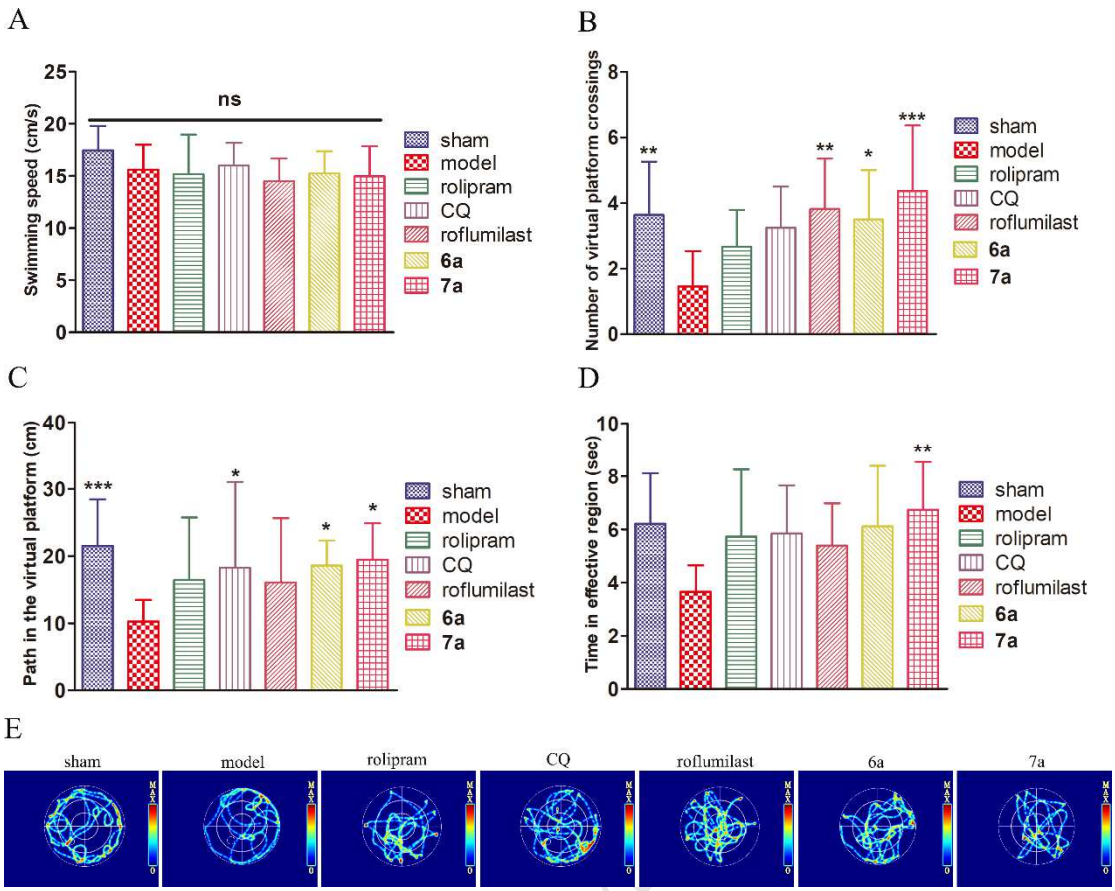

Figure 8. Effect of compounds **6a** and **7a** on the spatial probe trial in $A\beta_{25-35}$-induced learning and recognition dysfunction mice. Rolipram (4 mg/kg), roflumilast (4 mg/kg) and CQ (30 mg/kg) were used as references. The results are expressed as the mean ± SD. Student's t test: ∗ $p < 0.05$, ∗∗ $p < 0.01$, ∗∗∗ $p < 0.001$ versus the model group. Mean ± SD. (A) Swimming speed. (B) Number of virtual platform crossings. (C) Path in the virtual platform (D) Time in the effective region. (E) Representative tracks of the mice in the spatial probe trials. Student's t test: ∗ $p < 0.05$, ∗∗ $p < 0.01$, ∗∗∗ $p < 0.001$ versus the model group.

Histopathological studies in the hippocampus. Histopathological studies in the hippocampus were performed using hematoxylin and eosin (H&E) stain (Figure 9). The hippocampus neurons in the CA1, CA3 and dentate gyrus (DG) regions in the sham group were intact and properly aligned. Conversely, the neurons in the mice in the model group exhibited robust nuclear pyknosis and a reduction in the number of

neurons with noteworthy nuclear shrinkage, irregular array, much more darkly stained cells and neuronal loss, proving the success of model. In **7a**-treated mice, hippocampal neurons were markedly protected exhibited a nearly normal state. The hippocampal neurons in the rolipram, clioquinol, roflumilast and compound **6a** groups possessed a more normal morphology than the model group, however, **7a** produced a better protective effect on the hippocampal neurons than did the former compounds. The denatured cell index (DCI) in CA1, CA3 and DG region of the hippocampus is shown in Figure 10. It can be seen that **7a** remarkably reduced the ratio of apoptotic neurons in the CA1 (12.5 % ± 5.1), CA3 (7.9 % ± 5.4) and DG (18.7 % ± 4.8) regions, comparing to the model (40.6 % ± 12.5, 80.2 % ± 8.6, 55.8 % ± 7.2, respectively), rolipram (33.5 % ± 4.8, 41.1 % ± 9.3, 25.7 % ± 8.7, respectively), CQ (24.2 % ± 6.8, 37.8 % ± 8.6, 19.7 % ± 5.5, respectively), roflumilast (16.5 % ± 6.9, 38.7 % ± 4.3, 25.1 % ± 5.9) and compound **6a** (13.8 % ±5.1, 37.1 % ± 7.0, 26.8 % ± 6.9) groups.

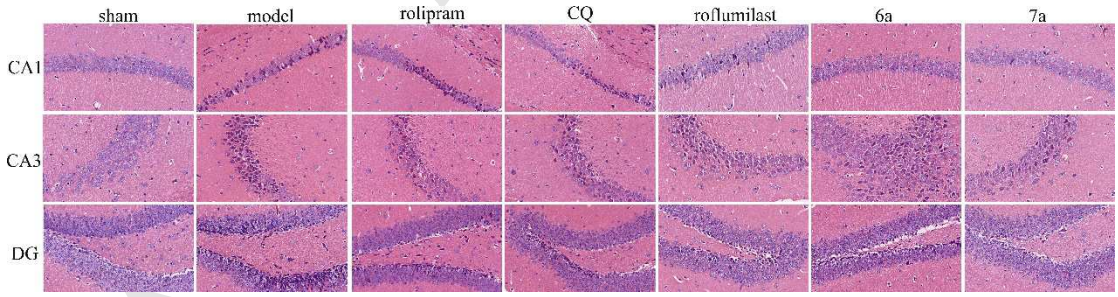

Figure 9. Histopathological examination in CA1, CA3 and DG regions of hippocampal (H&E stain ×200, n = 5, 400× magnification) for sham, model, rolipram, CQ, roflumilast, compounds 6a and 7a group.

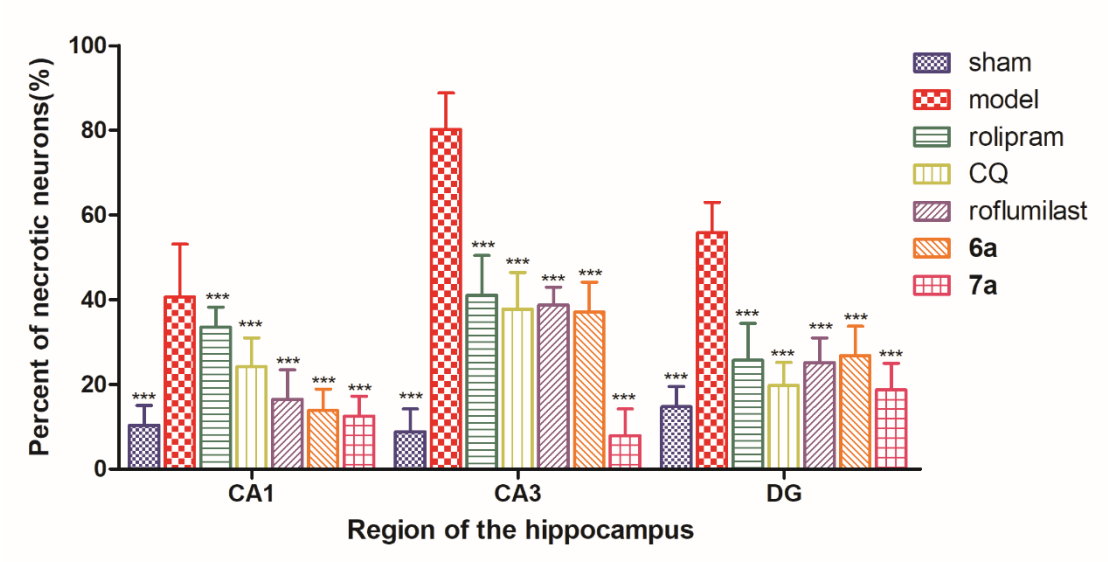

Figure 10. Denatured cell index (DCI) in CA1, CA3 and DG regions of mouse hippocampal neurons (DCI = denatured cells/total cells H&E stain, n = 5). These results are expressed as the means ± SD. Two-way ANOVA: *** $p < 0.001$ versus the model.

Conclusion.

Multitarget-directed ligands possess two or more complementary biological activities and may represent an important advance in treating the multifaceted conditions present in AD. Considering the importance of PDE4 inhibition and the modulation of biometals in AD therapeutics, we developed a series of novel compounds that possess the fragments of PDE4D (rolipram or roflumilast) and a modulator of metal-Aβ interactions (CQ). In vitro assays demonstrate that these hybrids have good PDE4D inhibitory activity, antioxidation properties, and the ability to modulate biometal ions. The structure-activity-relationship (SAR) studies revealed that substituents at 5-position of CQ are very important for PDE4D inhibitory activity. Compounds **6a** and **7a** exhibited effective PDE4D inhibitory potency, biometal chelating activities and modulation of metal-induced Aβ aggregation with improved BBB penetrability

and metabolic stability in rat liver microsomes. Finally, an oral intake of the optimal compounds **6a** and **7a** by AD mice induced by $A\beta_{25-35}$ demonstrated significant enhancements in cognitive and spatial memory performance in the Morris water-maze test. Remarkably, **7a** had better behavioral performance and could protect hippocampal neurons against Aβ toxicity. Other studies on the pharmaceutical properties of **7a** are in progress.

Experiment section

General chemistry. ^{1}H NMR and ^{13}C NMR was recorded on a Bruker Avance III spectrometer (400 or 500 MHz) with trimethylsilane as the internal standard. Melting points were measured in a SRS-Opti melting point apparatus. Reactions progress were monitored by thin-layer chromatography (TLC) with UV light (254 nm) for visualization. High-resolution mass spectra (HRMS) measurements were generated on a Shimadzu LCMS-IT-TOF mass instrument. HPLC analyses were carried out on an Agilent 1200 series using C18 column (Agilent ZORBAX Eclipse XDB-C18 5 μm. 4.6 mm × 250 mm column). The eluent was CH_3CN / H_2O = 90 / 10, at a flow rate of 0.5 mL/min and the purity was record at 254 nm. The purity of all new compounds was at least 95 %.

General procedures for the preparation of 2a-c, 3a-c and 4a-c. To a solution of 3,4-dimethoxybenzoic acid or 3-(cyclopentyloxy)-4-methoxybenzoic acid, or 3-(cyclopropylmethoxy)-4-(difluoromethoxy)benzoic acid in 10 mL of dichloromethane, thionyl chloride (15 mL) and N,N-dimethylformamide (0.5 mL)

were added. After the reaction mixture was heated at 85 °C for 3 h, the solvents were removed under vacuum to afford the corresponding acyl chloride which was used without any further purification. Acyl chloride (1.5 equiv.) in 2 mL of CH_2Cl_2 was added dropwise to a solution amino **1a**, **1b** or **1c** (1.0 equiv.), and triethylamine (10.0 equiv.) in 20 mL of CH_2Cl_2. The reaction mixture was stirred at room temperature for 16 h. The mixture was extracted with dichloromethane, washed with water, dried over Na_2SO_4, and concentrated under reduced pressure to afford the crude residue which was purified using column chromatography. (petroleum ether/ dichloromethane = 3 : 1)

Tert-butyl (5-(3,4-dimethoxybenzamido)quinolin-8-yl) carbonate (**2a**) Yellow solid, 56 % yield. ^{1}H NMR (400 MHz, $CDCl_3$) δ 8.95 – 8.87 (m, 1H), 8.23 (s, 1H), 8.15 (dd, *J* = 9.0, 7.6 Hz, 1H), 7.97 (s, 1H), 7.76 (s, 1H), 7.70 (d, *J* = 7.7 Hz, 1H), 7.43 (dd, *J* = 8.5, 4.1 Hz, 1H), 7.33 – 7.29 (q, J - 8.9 Hz, 1H), 2.39 (s, 6H), 1.65 (s, 9H).

Tert-butyl (5-(3,4-dimethoxybenzamido)-7-iodoquinolin-8-yl) carbonate (**2b**) Yellow solid, 58 % yield. ^{1}H NMR (400 MHz, $CDCl_3$) δ 8.97 (dd, *J* = 4.1, 1.5 Hz, 1H), 8.23 (dd, *J* = 8.6, 1.5 Hz, 1H), 8.09 (s, 1H), 7.87 (d, *J* = 8.2 Hz, 1H), 7.78 (s, 1H), 7.71 (d, *J* = 7.8 Hz, 1H), 7.56 (d, *J* = 8.2 Hz, 1H), 7.47 (dd, *J* = 8.6, 4.1 Hz, 1H), 7.30 (q, *J* = 7.9 Hz, 1H), 2.39 (s, 3H), 2.39 (s, 3H), 1.62 (s, 9H).

Tert-Butyl (5-(3-(cyclopentyloxy)-4-methoxybenzamido)quinolin-8-yl) carbonate (**3a**) Yellow solid, 64 % yield. ^{1}H NMR (400 MHz, DMSO-d_6) δ 10.58 (s, 1H), 9.11 (d, *J* = 4.1 Hz, 1H), 8.92 (d, *J* = 8.4 Hz, 1H), 8.01 (dd, *J* = 7.9, 5.1 Hz, 1H), 7.76 (dd, *J* = 13.6, 8.5 Hz, 2H), 7.69 (s, 1H), 7.57 (d, *J* = 8.1 Hz, 1H), 7.11 (d, *J* = 8.4 Hz, 1H), 4.93

(s, 1H), 1.92 (m, 2H), 1.75 (m, 4H), 1.59 (m, 2H). 1.66 (s, 9H).

Tert-Butyl (7-chloro-5-(3-(cyclopentyloxy)-4-methoxybenzamido)quinolin-8-yl) carbonate (**3b**) Yellow solid, 68 % yield. 1H NMR (400 MHz, $CDCl_3$) δ 8.92 (d, *J* = 3.9 Hz, 1H), 8.10 (d, *J* = 8.5 Hz, 1H), 8.06 (s, 1H), 7.81 (s, 1H), 7.54 (s, 1H), 7.48 (d, *J* = 8.4 Hz, 1H), 7.35 (dd, *J* = 8.5, 4.0 Hz, 1H), 6.92 (d, *J* = 8.3 Hz, 1H), 4.86 (s, 1H), 3.93 (s, 3H), 2.14 – 1.68 (m, 8H), 1.55 (s, 9H).

Tert-Butyl (5-(3-(cyclopentyloxy)-4-methoxybenzamido)-7-iodoquinolin-8-yl) carbonate (**3c**) Yellow solid, 65 % yield. 1H NMR (400 MHz, $CDCl_3$) δ 8.84 (d, *J* = 3.9 Hz, 1H), 8.09 (d, *J* = 13.2 Hz, 1H), 8.05 (d, *J* = 5.5 Hz, 2H), 7.53 (s, 1H), 7.48 (d, *J* = 8.3 Hz, 1H), 7.33 (dd, *J* = 8.4, 4.0 Hz, 1H), 6.90 (d, *J* = 8.3 Hz, 1H), 4.84 (s, 1H), 3.92 (s, 3H), 2.04 – 1.70 (m, 8H), 1.60 (s, 10H).

Tert-Butyl (5-(3-(cyclopropylmethoxy)-4-(difluoromethoxy)benzamido)quinolin-8-yl) carbonate (**4a**) Yellow solid, 67 % yield. 1H NMR (400 MHz, $CDCl_3$) δ 8.89 (dd, *J* = 4.1, 1.5 Hz, 1H), 8.30 (s, 1H), 8.04 (dd, *J* = 8.6, 1.5 Hz, 1H), 7.58 (dd, *J* = 4.9, 2.9 Hz, 2H), 7.47 – 7.40 (m, 2H), 7.35 (dd, *J* = 8.6, 4.1 Hz, 1H), 7.24 (d, *J* = 8.2 Hz, 1H), 6.75 (t, *J* = 75.0 Hz, 1H), 3.95 (d, *J* = 6.9 Hz, 2H), 1.61 (s, 9H), 0.71 – 0.64 (m, 2H), 0.39 (q, *J* = 4.8 Hz, 2H).

Tert-Butyl (7-chloro-5-(3-(cyclopropylmethoxy)-4-(difluoromethoxy)benzamido)quinolin-8-yl) carbonate (**4b**) Yellow solid, 70 % yield. ^{1}H NMR (400 MHz, $CDCl_3$) δ 8.84 (dd, *J* = 4.1, 1.6 Hz, 1H), 8.29 (s, 1H), 7.95 (dd, *J* = 8.5, 1.6 Hz, 1H), 7.55 (s, 1H), 7.52 (d, *J* = 1.9 Hz, 1H), 7.44 (dd, *J* = 8.3, 1.9 Hz, 1H), 7.26 (dd, *J* = 8.6, 4.1 Hz, 1H), 7.17 (d, *J* =

8.2 Hz, 1H), 6.99 – 6.54 (m, 1H), 3.90 (d, *J* = 6.9 Hz, 2H), 1.50 (s, 9H), 0.73 – 0.61 (m, 2H), 0.36 (q, *J* = 4.8 Hz, 2H).

Tert-butyl

(5-(3-(cyclopropylmethoxy)-4-(difluoromethoxy)benzamido)-7-iodoquinolin-8-yl) carbonate (**4c**) Yellow solid, 72 % yield. ^{1}H NMR (400 MHz, $CDCl_3$) δ 8.87 (dd, *J* = 4.1, 1.6 Hz, 1H), 8.11 (s, 1H), 8.06 (dd, *J* = 8.5, 1.6 Hz, 1H), 7.95 (s, 1H), 7.58 (d, *J* = 1.9 Hz, 1H), 7.44 (dd, *J* = 8.3, 1.9 Hz, 1H), 7.38 (dd, *J* = 8.5, 4.1 Hz, 1H), 7.24 (s, 1H), 6.73 (t, *J* = 74.9 Hz, 1H), 3.94 (d, *J* = 6.9 Hz, 2H), 1.60 (s, 9H), 0.73 – 0.57 (m, 2H), 0.44 – 0.27 (m, 2H).

General procedure for the preparation of 5a-b, 6a-c, 7a-c. A solution of 300 mg of **2a-c**, **3a-c** or **4a-c** in 12 mL dichloromethane was bubbled with HCl gas at room temperature for 6 h. The reaction mixture was filtered and dried under reduced pressure to yield the target product.

N-(8-Nydroxyquinolin-5-yl)-3,4-dimethoxybenzamide (**5a**) Yellow solid, 90 % yield. mp 215−216 °C. ^{1}H NMR (400 MHz, DMSO-d_6) δ 10.57 (s, 1H), 9.06 (dd, *J* = 4.6, 1.5 Hz, 1H), 8.67 (dd, *J* = 8.6, 1.4 Hz, 1H), 7.91 (s, 1H), 7.89 – 7.69 (m, 3H), 7.31 (d, *J* = 7.9 Hz, 1H), 2.33 (s, 3H), 2.32 (s, 3H). ^{13}C NMR (101 MHz, DMSO) δ 166.92, 148.12, 145.96, 141.15, 137.71, 136.82, 135.61, 131.79, 131.75, 129.90, 129.40, 126.85, 126.41, 125.93, 124.79, 122.28, 118.23, 19.90, 19.85. HRMS (ESI) m/z calcd for $C_{18}H_{16}N_2O_4$ $[M+Na]^+$, 347.1002; found, 347.0999. HPLC purity: 99.6 %, retention time:8.94 min.

N-(8-Hydroxy-7-iodoquinolin-5-yl)-3,4-dimethoxybenzamide (**5b**) Yellow solid, 90 %.

mp 215−216 °C. ^{1}H NMR (400 MHz, DMSO-d_6) δ 10.66 (s, 1H), 9.13 (dd, *J* = 5.1, 1.2 Hz, 1H), 8.99 (d, *J* = 8.6 Hz, 1H), 8.03 (dd, *J* = 8.7, 5.2 Hz, 1H), 7.94 (s, 1H), 7.87 (d, *J* = 7.8 Hz, 1H), 7.77 (dd, *J* = 8.4, 2.3 Hz, 1H), 7.63 (d, *J* = 8.4 Hz, 1H), 7.31 (d, *J* = 7.9 Hz, 1H), 2.33 (s, 3H), 2.32 (s, 3H). ^{13}C NMR (101 MHz, DMSO) δ 167.06, 147.54, 145.11, 142.63, 141.10, 136.80, 131.77, 131.73, 130.05, 129.89, 129.43, 128.13, 126.48, 126.44, 126.11, 125.94, 122.24, 115.63, 19.88, 19.83. HRMS (ESI) m/z calcd for $C_{18}H_{16}N_2O_4$ $[M+Na]^+$, 450.0066; found, 450.0076. HPLC purity: 98.8 %, retention time:6.41 min.

3-(Cyclopentyloxy)-N-(8-hydroxyquinolin-5-yl)-4-methoxybenzamide (**6a**) Yellow solid, 90 % yield. mp 196−197 °C. ^{1}H NMR (400 MHz, DMSO-d_6) δ 10.58 (s, 1H), 9.11 (d, *J* = 4.1 Hz, 1H), 8.92 (d, *J* = 8.4 Hz, 1H), 8.01 (dd, *J* = 7.9, 5.1 Hz, 1H), 7.76 (dd, *J* = 13.6, 8.5 Hz, 2H), 7.69 (s, 1H), 7.57 (d, *J* = 8.1 Hz, 1H), 7.11 (d, *J* = 8.4 Hz, 1H), 4.93 (s, 1H), 1.92 (m, 2H), 1.75 (m, 4H), 1.59 (m, 2H). ^{13}C NMR (101 MHz, DMSO-d_6) δ 166.48, 153.37, 147.80, 147.13, 145.33, 142.16, 128.17, 126.59, 126.32, 126.19, 126.05, 122.27, 121.98, 115.32, 114.83, 111.94, 80.41, 56.27, 32.74, 24.02. HRMS (ESI) m/z calcd for $C_{22}H_{22}N_2O_4$ $[M+H]^+$, 379.1652; found, 379.1643. HPLC purity: 96.8 %, retention time:11.97 min.

N-(7-Chloro-8-hydroxyquinolin-5-yl)-3-(cyclopentyloxy)-4-methoxybenzamide (**6b**) Yellow solid, 88% yield. mp 218−219 °C. ^{1}H NMR (400 MHz, DMSO-d_6) δ 10.54 (s, 1H), 9.05 (s, 1H), 8.60 (d, *J* = 8.0 Hz, 1H), 7.77 (s, 3H), 7.68 (s, 1H), 7.11 (d, *J* = 8.3 Hz, 1H), 4.93 (s, 1H), 3.85 (s, 3H), 1.93 (s, 2H), 1.74 (s, 4H), 1.59 (s, 2H). ^{13}C NMR (101 MHz, DMSO-d_6) δ 166.39, 153.29, 148.31, 147.07, 146.33, 137.38, 136.02,

127.08, 126.53, 126.29, 124.97, 122.31, 121.94, 117.93, 114.62, 111.83, 80.27, 56.22, 32.74, 24.07. HRMS (ESI) m/z calcd for $C_{22}H_{21}N_2O_4Cl[M+H]^+$, 413.1263; found, 413.1249. HPLC purity: 97.7 %, retention time:8.86 min.

3-(Cyclopentyloxy)-N-(8-hydroxy-7-iodoquinolin-5-yl)-4-methoxybenzamide (**6c**) Brown solid, 91 % yield. mp 185−186 °C. ^{1}H NMR (400 MHz, DMSO-d_6) δ 10.29 (s, 1H), 8.93 (d, *J* = 4.0 Hz, 1H), 8.35 (d, *J* = 8.5 Hz, 1H), 7.89 (s, 1H), 7.79 – 7.65 (m, 2H), 7.63 (s, 1H), 7.10 (d, *J* = 8.5 Hz, 1H), 4.90 (s, 1H), 3.85 (s, 3H), 1.93 (dd, *J* = 11.9, 6.5 Hz, 2H), 1.76 (d, *J* = 10.2 Hz, 4H), 1.65 – 1.47 (m, 2H). ^{13}C NMR (101 MHz, DMSO-d_6) δ 166.35, 153.22, 152.22, 148.94, 147.10, 136.77, 134.64, 134.12, 126.54, 126.48, 125.72, 122.48, 121.77, 114.60, 111.90, 80.32, 56.23, 32.74, 24.04. HRMS (ESI) m/z calcd for $C_{22}H_{21}N_2O_4I[M+H]^+$, 505.0619; found, 505.0597. HPLC purity: 99.8 %, retention time:14.4 min.

3-(Cyclopropylmethoxy)-4-(difluoromethoxy)-N-(8-hydroxyquinolin-5-yl)benzamide (**7a**) Yellow solid, 89 % yield. mp 187−188 °C. ^{1}H NMR (400 MHz, DMSO-d_6) δ 10.85 (s, 1H), 9.12 (dd, *J* = 5.1, 1.3 Hz, 1H), 8.96 (dd, *J* = 8.6, 1.0 Hz, 1H), 8.02 (dd, *J* = 8.7, 5.1 Hz, 1H), 7.95 – 7.89 (m, 1H), 7.75 (dd, *J* = 8.4, 2.0 Hz, 2H), 7.61 (d, *J* = 8.3 Hz, 1H), 7.35 (d, *J* = 8.3 Hz, 1H), 7.25 (t, J = 74.2 Hz, 1H), 4.05 (d, *J* = 7.0 Hz, 2H), 1.30 (ddt, *J* = 10.1, 7.1, 3.6 Hz, 1H), 0.68 – 0.53 (m, 2H), 0.50 – 0.32 (m, 2H). ^{13}C NMR (101 MHz, DMSO) δ 165.50, 149.50, 147.49, 144.85, 142.55, 142.52, 142.49, 141.82, 131.65, 131.60, 129.96, 127.81, 126.01, 125.27, 125.11, 121.84, 120.93, 120.26, 119.03, 116.46, 114.93, 114.10, 113.89, 73.41, 9.95, 3.02. HRMS (ESI) m/z calcd for $C_{21}H_{18}N_2O_4F_2[M+H]^+$, 401.1307; found, 401.1293. HPLC purity:

99.3 %, retention time:11.8 min.

N-(7-Chloro-8-hydroxyquinolin-5-yl)-3-(cyclopropylmethoxy)-4-(difluoromethoxy) benzamide (**7b**) Yellow green solid, 89 % yield. mp 230−231 °C. ^{1}H NMR (400 MHz, DMSO-d_6) δ 10.68 (s, 1H), 9.02 (d, *J* = 4.0 Hz, 1H), 8.55 (d, *J* = 8.5 Hz, 1H), 7.86 (s, 1H), 7.80 – 7.70 (m, 3H), 7.35 (d, *J* = 8.3 Hz, 1H), 7.25 (t, J = 74.1 Hz, 1H), 4.03 (d, *J* = 6.9 Hz, 2H), 1.39 – 1.22 (m, 1H), 0.61 (q, *J* = 4.9 Hz, 2H), 0.38 (t, *J* = 4.7 Hz, 2H). ^{13}C NMR (101 MHz, DMSO-d_6) δ 165.94, 149.98, 148.69, 147.10, 142.97, 136.80, 136.38, 132.22, 126.99, 125.90, 124.82, 122.37, 121.33, 120.75, 119.55, 117.27, 116.98, 114.43, 73.84, 10.45, 3.54. HRMS (ESI) m/z calcd for $C_{21}H_{17}N_2O_4F_2Cl$ $[M+H]^+$, 435.0921; found, 435.0918. HPLC purity: 98.1 %, retention time:7.86 min.

3-(Cyclopropylmethoxy)-4-(difluoromethoxy)-N-(8-hydroxy-7-iodoquinolin-5-yl)benza mide (**7c**) Yellow solid, 89 % yield. mp 198−199 °C. ^{1}H NMR (400 MHz, DMSO-d_6) δ 10.63 (s, 1H), 8.98 (d, *J* = 4.2 Hz, 1H), 8.48 (d, *J* = 8.5 Hz, 1H), 7.96 (s, 1H), 7.86 (s, 1H), 7.81 – 7.64 (m, 2H), 7.35 (d, *J* = 8.3 Hz, 1H), 7.25 (t, J = 74.2 Hz, 1H), 4.03 (d, *J* = 7.0 Hz, 2H), 1.38 – 1.24 (m, 1H), 0.74 – 0.50 (m, 2H), 0.38 (q, *J* = 4.8 Hz, 2H). ^{13}C NMR (101 MHz, DMSO-d_6) δ 165.93, 151.64, 149.97, 148.50, 142.93, 136.06, 135.67, 134.55, 132.26, 126.47, 125.73, 122.54, 121.29, 120.75, 119.55, 116.98, 114.40, 73.83, 10.45, 3.55. HPLC purity: 98.1 %, retention time:8.25 min.

General procedures for the preparation of 9a and 9b. To a solution of **8a** or **8b** (50 mmol) in acetone (150 mL), benzyl bromide (10.3 g, 60 mmol), and K_2CO_3 (13.8 g, 100 mmol) were added with stirring. The resulting mixture was refluxed for 5 h. The mixture was cooled to room temperature and the solvent was removed in vacuum. The

residue was added water (100 mL) and extracted with ethyl acetate. The extract was washed with saturated Na_2CO_3, water and brine successively. The organic layer was dried over Na_2SO_4 and concentrated in vacuo to give the benzyl-protected crude product, which was purified by silica-column chromatography.

8-(Benzyloxy)-2-methylquinoline Pale yellow solid, 89 % yield. (petroleum / EtOAc = 8 / 1) ^{1}H NMR (400 MHz, $CDCl_3$): 8.03 (d, *J* = 8.4 Hz, 1H), 7.52–7.58 (m, 2H), 7.28–7.42 (m, 6H), 7.02 (dd, ^3J = 7.6 Hz, ^4J = 1.5 Hz, 1H), 5.49 (s, 2H), d = 2.84 (s, 3H).

8-(Benzyloxy)-5,7-dichloro-2-methylquinoline Yellow solid, 91 % yield. (petroleum/EtOAc = 10/1) ^{1}H NMR (400 MHz, $CDCl_3$): 8.38 (d, *J* = 8.4, 1H), 7.63 (d, *J* = 6.8, 2H), 7.55 (s, 1H), 7.44-7.30 (m, 4H), 5.46 (s, 2H), 2.81 (s, 3H).

General procedures for the preparation of 10a and 10b. Compound **9a** or **9b** (40.0 mmol) and SeO_2 (49.9 mmol) were suspended in dioxane (100 mL). After the mixture was heated at 80 °C for 2 h, the suspension was cooled to room temperature, filtered through Celite and washed with dichloromethane. The filtrate was evaporated to afford the crude product which was purified by column chromatography to give the desired compound (petroleum / EtOAc = 4 / 1). A solution of sodium chlorite (12.5 mmol) in NaH_2PO_4 buffer (10 mL, pH 3.5) was added dropwise to a rapidly stirred solution of aldehyde (10 mmol) and 2-methyl-2-butene (100 mmol) in t-BuOH (50 mL) at room temperature. After stirred at ambient temperature for 8 hours, the mixture was extracted with ethyl acetate. The organic layer was washed with water (25 mL) and brine (25 mL). Drying and removal of solvents afforded white solid which was used without any further purification.

8-Hydroxyquinoline-2-carboxylic acid (**10a**) White solid, 91 % yield. ^{1}H NMR (400 MHz, $CDCl_3$) δ 8.40 (d, *J* = 8.4 Hz, 1H), 8.32 (d, *J* = 8.4 Hz, 1H), 7.37–7.65 (m, 7H), 7.24 (dd, ^{3}J = 7.8 Hz, ^{4}J = 1.2 Hz, 1H), 5.38 (s, 2H).

5,7-Dichloro-8-hydroxyquinoline-2-carboxylic acid (**10b**) Faint yellow solid, 87 % yield. ^{1}H NMR (400 MHz, DMSO-d_6) δ 8.71 (d, *J* = 8.8 Hz, 1H), 8.29 (d, *J* = 8.8 Hz, 1H), 8.06 (s, 1H), 7.62 (d, *J* = 6.9 Hz, 2H), 7.46 – 7.30 (m, 3H), 5.60 (s, 2H).

General Procedures for the Preparation of 11a-b and 12a-b. To a mixture of thionyl chloride (8 mL) and DMF (0.05 mL), compound **10a** or **10b** (2 mmol) were added. After the mixtures were stirred at 85 °C for 3 h, the solvent was evaporated under a vacuum to afford the crude acyl chloride which was used for next step without any further purification. To a stirred solution of the corresponding amine (2 mmol) in anhydrous CH_2Cl_2 containing dry triethylamine (5 mmol), the above acyl chloride (2.1 mmol) in anhydrous CH_2Cl_2 (12 mL) was added dropwise over 15 min at 0 °C. After the mixture was stirred for 4 h at room temperature, water was added, and then extracted with CH_2Cl_2, dried, and concentrated under vacuum to produce the crude products, which were purified by column chromatography using silica gel. (petroleum / EtOAc = 4 / 1)

8-(Benzyloxy)- N-(3,4-dimethoxyphenyl)quinoline-2-carboxamide (**11a**) Yellow oil, 66 % yield. ^{1}H NMR (400 MHz, $CDCl_3$) δ 10.34 (s, 1H), 8.36 (dd, *J* = 26.7, 8.5 Hz, 2H), 7.64 (d, *J* = 7.3 Hz, 2H), 7.59 (d, *J* = 2.4 Hz, 1H), 7.57 – 7.42 (m, 4H), 7.38 (t, *J* = 7.3 Hz, 1H), 7.21 (dd, *J* = 7.5, 1.2 Hz, 1H), 7.16 (dd, *J* = 8.6, 2.4 Hz, 1H), 6.88 (d, *J* = 8.6 Hz, 1H), 5.38 (s, 2H), 3.92 (s, 3H), 3.90 (s, 3H).

8-(Benzyloxy)-5,7-dichloro-N-(3,4-dimethoxyphenyl)quinoline-2-carboxamide (**11b**) Yellow oil, 71 % yield. ^{1}H NMR (400 MHz, $CDCl_3$) δ 9.86 (s, 1H), 8.61 (dd, *J* = 103.7, 8.7 Hz, 2H), 7.76 (s, 1H), 7.64 (d, *J* = 7.0 Hz, 2H), 7.53 (s, 1H), 7.48 – 7.30 (m, 3H), 6.90 – 6.78 (m, 2H), 5.40 (s, 2H), 3.90 (s, 3H), 3.89 (s, 3H).

8-(Benzyloxy)-N-(3-(cyclopentyloxy)-4-methoxyphenyl)quinoline-2-carboxamide (**12a**) Yellow oil, 69 % yield. ^{1}H NMR (400 MHz, $CDCl_3$) δ 10.34 (s, 1H), 8.36 (dd, *J* = 26.7, 8.5 Hz, 2H), 7.64 (d, *J* = 7.3 Hz, 2H), 7.59 (d, *J* = 2.4 Hz, 1H), 7.57 – 7.42 (m, 4H), 7.38 (t, *J* = 7.3 Hz, 1H), 7.21 (dd, *J* = 7.5, 1.2 Hz, 1H), 7.16 (dd, *J* = 8.6, 2.4 Hz, 1H), 6.88 (d, *J* = 8.6 Hz, 1H), 4.90 (s, 1H), 1.93 (m, 2H), 1.74 (m, 4H), 1.60 (m, 2H).

8-(Benzyloxy)-5,7-dichloro-N-(3-(cyclopentyloxy)-4-methoxyphenyl)quinoline-2-carb oxamide (**12b**) White solid, 71 % yield. ^{1}H NMR (400 MHz, $CDCl_3$) δ 9.83 (s, 1H), 8.60 (dd, *J* = 98.7, 8.7 Hz, 2H), 7.75 (s, 1H), 7.66 – 7.60 (m, 2H), 7.55 (s, 1H), 7.40 (ddd, *J* = 9.9, 7.4, 5.9 Hz, 3H), 6.82 (d, *J* = 1.3 Hz, 2H), 5.40 (s, 2H), 4.86 – 4.72 (m, 1H), 3.86 (s, 3H), 2.20 – 1.69 (m, 6H), 1.63 – 1.55 (m, 2H).

General procedures for the preparation of 13a-b, 14a-b. To a solution of **11a-b**, or **12a-b** (2 mmol) in 20 mL of MeOH, Pd / C (0.10 g, 10 %) was added. The reaction mixture was stirred under H_2 atmosphere for 12 h. After Pd / C was filtered off, the filtrate was concentrated under vacuum, and the residue was purified by flash column chromatography to give product (petroleum / EtOAc = 2 / 1).

N-(3,4-Dimethoxyphenyl)-8-hydroxyquinoline-2-carboxamide (**13a**) White solid, 64 %. mp 178−179 °C. ^{1}H NMR (400 MHz, DMSO-d_6) δ 11.17 (s, 1H), 8.57 (d, *J* = 8.5 Hz, 1H), 8.27 (d, *J* = 8.5 Hz, 1H), 7.65 (s, 1H), 7.61 (t, *J* = 7.9 Hz, 1H), 7.51 (dd,

J = 16.3, 8.5 Hz, 1H), 7.24 (d, *J* = 7.5 Hz, 1H), 7.02 (t, *J* = 10.5 Hz, 1H), 3.83 (d, *J* = 10.5 Hz, 1H), 3.79 (s, 1H). ^{13}C NMR (101 MHz, DMSO-d_6) δ 162.30, 154.20, 149.04, 147.98, 145.97, 138.51, 136.87, 132.30, 130.10, 119.38, 118.10, 113.26, 112.51, 112.39, 106.23, 106.14, 56.19, 56.02. HRMS (ESI) m/z calcd for $C_{18}H_{14}N_2O_4Cl_2$ $[M-H]^-$, 323.1037; found, 323.1040. HPLC purity: 99.6 %, retention time:8.70 min.

5,7-Dichloro-N-(3,4-dimethoxyphenyl)-8-hydroxyquinoline-2-carboxamide (**13b**)

White solid, 54 % yield. mp 143−144 °C. ^{1}H NMR (400 MHz, DMSO-d_6) δ 11.19 (s, 1H), 8.66 (d, *J* = 8.8 Hz, 1H), 8.37 (d, *J* = 8.8 Hz, 1H), 7.89 (s, 1H), 7.67 – 7.60 (m, 1H), 7.53 – 7.41 (m, 1H), 7.00 (d, *J* = 8.7 Hz, 1H), 3.82 (s, 3H), 3.78 (s, 3H). ^{13}C NMR (101 MHz, DMSO-d_6) δ 161.52, 150.04, 149.56, 149.03, 146.13, 137.55, 135.40, 132.11, 129.88, 126.15, 120.74, 119.52, 116.60, 113.44, 112.39, 106.45, 56.20, 56.05. HRMS (ESI) m/z calcd for $C_{18}H_{14}N_2O_4Cl_2$ $[M+Na]^+$, 415.0223; found, 415.0228. HPLC purity: 96.1 %, retention time:9.68 min.

N-(3-(Cyclopentyloxy)-4-methoxyphenyl)-8-hydroxyquinoline-2-carboxamide (**14a**)

White solid, Yield 77%. mp 215−216 °C. ^{1}H NMR (400 MHz, $CDCl_3$) δ 9.95 – 9.81 (m, 1H), 8.47 – 8.38 (m, 1H), 8.33 (t, *J* = 7.5 Hz, 1H), 8.20 (s, 1H), 7.59 – 7.48 (m, 1H), 7.41 (d, *J* = 8.2 Hz, 1H), 7.30 – 7.23 (m, 1H), 7.13 (dt, *J* = 11.2, 5.6 Hz, 1H), 6.82 – 6.72 (m, 1H), 4.77 – 4.65 (m, 1H), 3.84 – 3.73 (m, 1H), 1.93 – 1.80 (m, 1H), 1.79 – 1.71 (m, 1H), 1.58 – 1.45 (m, 1H). ^{13}C NMR (101 MHz, $CDCl_3$) δ 161.93, 152.30, 148.19, 147.88, 147.07, 138.06, 136.48, 130.97, 129.82, 129.51, 119.74, 118.37, 112.40, 112.20, 111.59, 108.16, 80.46, 56.26, 32.78, 24.04. HRMS (ESI) m/z calcd for $C_{22}H_{22}N_2O_4$ $[M-H]^-$, 377.1507; found, 377.1525. HPLC purity: 96.3 %,

retention time:9.43 min.

5,7-Dichloro-N-(3-(cyclopentyloxy)-4-methoxyphenyl)-8-hydroxyquinoline-2-carboxa mide (**14b**) White solid, 77 % yield. mp 149−150 °C. ^{1}H NMR (400 MHz, $CDCl_3$) δ 10.22 (s, 1H), 9.44 (s, 1H), 8.53 (s, 2H), 7.61 (s, 1H), 7.28 (s, 1H), 7.09 (d, *J* = 8.9 Hz, 1H), 6.54 (d, *J* = 8.7 Hz, 1H), 4.37 (s, 1H), 3.71 (s, 3H), 1.55 – 1.06 (m, 6H), 0.88 (d, *J* = 6.7 Hz, 2H). ^{13}C NMR (101 MHz, $CDCl_3$) δ 161.58, 149.47, 147.70, 147.49, 147.15, 136.79, 135.27, 130.50, 129.72, 125.92, 121.43, 120.49, 117.04, 112.87, 111.78, 108.23, 80.18, 56.00, 32.61, 23.91. HRMS (ESI) m/z calcd for $C_{22}H_{20}N_2O_4Cl_2[M+H]^+$, 447.0873; found, 447.0890. HPLC purity: 97.1 %, retention time:9.41 min.

General procedures for the preparation of 17a-b. To a solution of 3,4-dimethoxybenzoic acid or 3-(cyclopentyloxy)-4-methoxybenzoic acid or 3-(cyclopropylmethoxy)-4-(difluoromethoxy)benzoic acid in 10 mL of dichloromethane , thionyl chloride (20 mL) and DMF (0.5 mL, as a catalyst) was added. After the reaction mixture was stirred at reflux for 3 h, the solvents were evaporated under vacuum to afford the crude acyl chloride which was used without further purification. To a solution of 20 mL of anhydrous dichloromethane, 10.0 equiv. of anhydrous triethylamine and 1.0 equiv. of compound **16**, the corresponding acyl chloride (1.5 equiv.) in 2 mL of anhydrous dichloromethane was added dropwise. After the reaction mixture was stirred at room temperature for 16 h, saturated $NaHCO_3$ was added, and then extracted with dichloromethane. The organic phase was washed with brine, dried over anhydrous Na_2SO_4, and concentrated under reduced

pressure to afford the crude product which was purified using column chromatography (petroleum / EtOAc = 3 / 1).

N-(8-((Tert-butyldimethylsilyl)oxy)quinolin-2-yl)-3-(cyclopentyloxy)-4-methoxybenzamide (**17a**) Colorless oil, 60 % yield. ^{1}H NMR (400 MHz, $CDCl_3$) δ 8.51 (d, *J* = 7.5 Hz, 1H), 8.17 (d, *J* = 9.0 Hz, 1H), 7.76 (s, 1H), 7.69 (d, *J* = 7.7 Hz, 1H), 7.40 (dd, *J* = 8.1, 1.2 Hz, 1H), 7.35 – 7.25 (m, 2H), 7.14 (dd, *J* = 7.6, 1.3 Hz, 1H), 2.36 (s, 3H), 2.34 (s, 3H), 1.10 (s, 9H), 0.28 (s, 6H).

*N-(8-((Tert-butyldimethylsilyl)oxy)quinolin-2-yl)-3-(cyclopropylmethoxy)-4-(difluoromethoxy)benzamide (***17b***)* Colorless oil, 64 % yield. ^{1}H NMR (400 MHz, $CDCl_3$) δ 8.65 (d, *J* = 117.1 Hz, 2H), 8.20 (d, *J* = 8.8 Hz, 1H), 7.66 (d, *J* = 7.4 Hz, 1H), 7.52 (s, 1H), 7.43 (d, *J* = 8.0 Hz, 1H), 7.34 (dd, *J* = 16.5, 8.3 Hz, 2H), 7.17 (dd, *J* = 7.6, 1.1 Hz, 1H), 6.76 (t, *J* = 75.0 Hz, 1H), 4.02 (d, *J* = 6.9 Hz, 2H), 1.13 (s, 9H), 0.71 (dt, *J* = 5.9, 5.4 Hz, 2H), 0.45 – 0.37 (m, 2H), 0.31 (s, 6H).

General procedures for the preparation of 18a-c. To a solution of **17a**, or **17b** (2 mmol) in THF (10 mL), 1 M solution of tetrabutylammonium fluoride in THF (3 mL, 3 mmol) was added at room temperature. After the solution was stirred for 2 h, the solvent was removed in reduced pressure and the residue was dissolved with EtOAc. The above solution was washed with H_2O and dried over Na_2SO_4. The solvent was evaporated in vacuum to give the crude product which was chromatographed over silica gel using dichloromethane / CH_3OH solution to give the product (dichloromethane / CH_3OH = 40 / 1).

3-(Cyclopentyloxy)-N-(8-hydroxyquinolin-2-yl)-4-methoxybenzamide (**18a**) White

solid, 89 % yield. mp 176-177 °C. ^{1}H NMR (400 MHz, DMSO-d_6) δ 10.69 (s, 1H), 9.27 (s, 1H), 8.33 (d, *J* = 9.0 Hz, 1H), 8.26 (d, *J* = 8.9 Hz, 1H), 7.75 (dd, *J* = 8.4, 2.1 Hz, 1H), 7.68 (d, *J* = 2.0 Hz, 1H), 7.46 – 7.36 (m, 1H), 7.33 (q, *J* = 8.1 Hz, 1H), 7.15 – 7.02 (m, 2H), 5.23 – 4.65 (m, 1H), 3.85 (s, 3H), 2.04 – 1.86 (m, 2H), 1.82 – 1.67 (m, 4H), 1.67 – 1.52 (m, 2H). ^{13}C NMR (101 MHz, DMSO-d_6) δ 169.33, 154.99, 150.25, 147.56, 147.30, 145.62, 128.62, 125.72, 123.65, 123.53, 118.67, 116.31, 115.32, 114.72, 111.90, 80.36, 56.35, 32.67, 24.09. HRMS (ESI) m/z calcd for $C_{22}H_{22}N_2O_4$ $[M+H]^+$, 379.1652; found, 379.1664. HPLC purity: 98.8 %, retention time:6.41 min.

3-(Cyclopropylmethoxy)-4-(difluoromethoxy)-N-(8-hydroxyquinolin-2-yl)benzamide (**18b**) White solid, 91 % yield. mp 162−163 °C. ^{1}H NMR (400 MHz, DMSO-d_6) δ 8.86 (t, *J* = 14.4 Hz, 1H), 8.43 (dd, *J* = 19.8, 9.3 Hz, 1H), 8.10 (d, *J* = 1.9 Hz, 1H), 7.91 (dt, *J* = 20.8, 10.4 Hz, 1H), 7.63 – 7.56 (m, 1H), 7.48 – 7.44 (m, 1H), 7.41 (d, *J* = 8.4 Hz, 1H), 7.31 (t, *J* = 73.8 Hz 1H), 4.11 (d, *J* = 7.0 Hz, 2H), 1.43 – 1.12 (m, 1H), 0.70 – 0.54 (m, 2H), 0.51 – 0.31 (m, 2H). ^{13}C NMR (101 MHz, DMSO-d_6) δ 168.61, 149.95, 147.87, 145.37, 144.52 (t, *J* = 3.1 Hz), 129.62, 128.62, 125.99, 122.58, 120.46, 119.36, 118.73, 116.79, 116.06, 115.36, 115.27, 114.21, 74.17, 10.39, 3.54. HRMS (ESI) m/z calcd for $C_{21}H18N_2O_4F_2$ $[M+H]^+$, 401.1307; found, 401.1327. HPLC purity: 98.9 %, retention time:10.66 min.

PDE4D inhibitory screening assay, oxygen radical absorbance capacity (ORAC-FL) assay. Blood–brain barrier (BBB) permeation assay, Metal-chelating study, ThT assay, Metabolic stability study, MTT assay and Intracellular antioxidant activity in SH-SY5Y cells assay.[39, 48] These assays

were performed in accordance with the previously reported procedures and described in the Supporting Information.

Ascorbate studies[42]. Compound **6a** and **7a** (50 μM, final concentration) were dissolved in methanol and diluted in 20 mM PBS (pH = 7.4). $CuSO_4$ (100 μM, final concentration) was dissolved in water and diluted in PBS. Ascorbate was diluted to the final concentration of 300 μM. Deferoxamine mesylate and coumarin-3-carboxylic acid (CCA) were prepared in PBS to final concentrations of 20 μM and 500 μM with a final sample volume of 200 μL. The mixture of the compound (60 μL), $CuSO_4$ (10 μL), Deferoxamine mesylate (10 μL) and CCA (20 μL) was pre-incubated for 10 min, and then ascorbate (100 μL) was added and mixed up. The fluorescence was recorded every 30 second for 15 min at 37 °C (excitation, 395 nm; emission, 450 nm).

TEM Assay.[49] The samples were prepared by the same procedure as the ThT assay. Aliquots (10 μL) of the samples were placed on a carbon-coated copper grid for 2 min. Each grid was stained with 3% phosphotungstic acid for 2 min. After draining off the excess staining solution, pure water was added and drained off again with the filter paper. The specimen was transferred into a transmission electron microscope (Hitachi H-7650).

Molecular docking studies. All computational work was performed using Schrodinger Suites 2015 under Windows7 O.S. The PDE4D protein (1XOQ) and ligands (**6a**, **7a** and roflumilast) were performed using the protein and ligand preparation utilities. Various conformations of **6a** and **7a** were obtained for docking

studies. The docking studies were determined using the SP mode and the default parameters of Glide. The docking results for the best docking score of compound **6a** and **7a** are extracted for molecular binding mode analysis.

Acute toxicity assay, **Cognitive and memory improvement in a mouse model of AD, Hematoxylin and eosin (H&E) stain and histopathological.**[50-52] These assays were performed in accordance with the previously reported procedures and described in the Supporting Information.

Supporting information

^{1}H and ^{13}C NMR spectra, HPLC chromatograms, PDE4D inhibitory screening assay, oxygen radical absorbance capacity (ORAC-FL) assay. Blood–brain barrier (BBB) permeation assay, Metal-chelating study, ThT assay, Metabolic stability study, MTT assay and Intracellular antioxidant activity in SH-SY5Y cells assay. Acute toxicity assay, Cognitive and memory improvement in a mouse model of AD, Hematoxylin and eosin (H&E) stain and histopathological.

Abbreviations

AD, Alzheimer's disease; ROS, reactive oxygen species; PDE4D, phosphodiesterase 4D; BBB, blood-brain barrier; Aβ, beta amyloid protein; MTDLs, multitarget-directed ligands; MWM, Morris water-maze test; SAR, structure−activity relationship; ORAC, free oxygen radical absorbance capacity; UV-vis, ultraviolet–visible; CNS, central nervous system; PAMPA, parallel artificial membrane permeation assay; DCFH-DA,

2',7'-dichlorofluorescein diacetate; CQ, clioquinol; ThT, thioflavin T; TEM, transmission electron microscope; ROF, roflumilast; HEPES, 2-[4-(2-hydroxyethyl)piperazin-1-yl] ethanesulfonic acid; MTT, 3-(4,5-dimethyl-2-thiazolyl)-2,5-diphenyl-2-H-tetrazolium bromide; ICV, intracerebroventricular injections; H&E, hematoxylin and eosin.

Corresponding authors

*For L.H.: phone, +086-20-3994-3051; fax, +086-20-3994-3051; e-mail, huangl72@mail.sysu.edu.cn. For X.L.: phone, +086-20-3994-3050; fax, +086-20-3994-3050; e-mail, lixsh@mail.sysu.edu.cn.

Acknowledgments

We thank the National Natural Science Foundation of China (Grants 21772241 and 21302235), Guangdong High-Level Personnel of Special Support Program-Young Top-Notch Talent Project (Grant 2015TQ01R244) and The Guangzhou Pearl River New Star Fund Science and Technology Planning Project (Grant 201610010111) for financial support of this study.

References

[1] B.E. Stopschinski, M.I. Diamond, The prion model for progression and diversity of neurodegenerative diseases, Lancet Neurol. 16 (2017) 323-332.

[2] A.C. Herrera, M. Prince, M. Knapp, M. Karagiannidou, M. Guerchet, World Alzheimer Report 2016: Improving healthcare for people with dementia. Coverage, quality and costs now and in the future, (2016).

[3] K. Iqbal, I. Grundke-Iqbal, Alzheimer's disease, a multifactorial disorder seeking multitherapies, Alzheimers Dement. 6 (2010) 420-424.

[4] G. Pepeu, M.G. Giovannini, Cholinesterase inhibitors and beyond, Curr. Alzheimer Res. 6 (2009) 86-96.

[5] J.B. Torres, E.M. Andreozzi, J.T. Dunn, M. Siddique, I. Szanda, D.R. Howlett, K. Sunassee, P.J. Blower, PET imaging of copper trafficking in a mouse model of Alzheimer disease, J. Nucl. Med. 57 (2016) 109-114.

[6] Z. Lv, M.M. Condron, D.B. Teplow, Y.L. Lyubchenko, Nanoprobing of the effect of Cu^{2+} cations on misfolding, interaction and aggregation of amyloid β peptide, J. Neuroimmune Pharm. 8 (2013) 262-273.

[7] S. Jun, J.R. Gillespie, B. Shin, S. Saxena, The second Cu(II)-binding site in a proton-rich environment interferes with the aggregation of amyloid-β(1−40) into amyloid fibrils, Biochemistry 48 (2009) 10724-10732.

[8] S. Parthasarathy, B. Yoo, D. Mcelheny, W. Tay, Y. Ishii, Capturing a reactive state of amyloid aggregates: NMR-based characterization of copper-bound Alzheimer disease amyloid β-fibrils in a redox cycle, J. Biol. Chem. 289 (2014) 9998-10010.

[9] E. Atrián-Blasco, E. Cerrada, A. Conte-Daban, D. Testemale, P. Faller, M. Laguna, C. Hureau, Copper(I) targeting in the Alzheimer's disease context: a first example using the biocompatible PTA ligand, Metallomics, 7 (2015) 1229-1232.

[10] R. Deloncle, O. Guillard, Is brain copper deficiency in Alzheimer's, Lewy body, and Creutzfeldt Jakob diseases the common key for a free radical mechanism and oxidative stress-induced damage?, J. Alzheimers Dis. 43 (2015) 1149-1156.

[11] S.C. Drew, The case for abandoning therapeutic chelation of copper ions in Alzheimer's disease, Front. Neurosci. 11 (2017) 317-321.

[12] F. Tahmasebinia, S. Emadi, Effect of metal chelators on the aggregation of beta-amyloid peptides in the presence of copper and iron, Biometals, 30 (2017) 285-293.

[13] V. Lanza, D. Milardi, G. Di Natale, G. Pappalardo, Repurposing of copper(II)-chelating drugs for the treatment of neurodegenerative diseases, Curr. Med. Chem. 25 (2017) 525-539.

[14] F. Prati, C. Bergamini, R. Fato, O. Soukup, J. Korabecny, V. Andrisano, M. Bartolini, M.L. Bolognesi, Novel 8-hydroxyquinoline derivatives as multitarget compounds for the treatment of Alzheimer's disease, ChemMedChem 11 (2016) 1284-1295.

[15] X. Li, H. Wang, Z. Lu, X. Zheng, W. Ni, J. Zhu, Y. Fu, F. Lian, N. Zhang, J. Li, H. Zhang, F. Mao, Development of multifunctional pyrimidinylthiourea derivatives as potential anti-Alzheimer agents, J. Med. Chem. 59 (2016) 8326-8344.

[16] D.F. Tardiff, L.E. Brown, X. Yan, R. Trilles, N.T. Jui, M.I. Barrasa, K.A. Caldwell, G.A. Caldwell, S.E. Schaus, S. Lindquist, Dihydropyrimidine-thiones and clioquinol synergize to target β-amyloid cellular pathologies through a metal-dependent mechanism, ACS Chem. Neurosci. 8 (2017) 2039-2055.

[17] M. Dong, H. Li, D. Hu, W. Zhao, X. Zhu, H. Ai, Molecular dynamics study on the inhibition mechanisms of drugs $CQ_{1–3}$ for Alzheimer amyloid-β_{40} aggregation induced by Cu^{2+}, ACS Chem. Neurosci. 7 (2016) 599-614.

[18] Zheng H, Gal S, Weiner LM, Bar-Am O, Warshawsky A, Fridkin M, Youdim MB. Novel multifunctional neuroprotective iron chelator-monoamine oxidase inhibitor drugs for neurodegenerative diseases: in vitro studies on antioxidant activity, prevention of lipid peroxide formation and monoamine oxidase inhibition. J. Neurochem. 95 (2005) 68–78.

[19] D. Antequera, M. Bolos, C. Spuch, C. Pascual, I. Ferrer, M.I. Fernandez-Bachiller, M.I. Rodríguez-Franco, E. Carro, Effects of a tacrine-8-hydroxyquinoline hybrid (IQM-622) on Aβ accumulation and cell death: Involvement in hippocampal neuronal loss in Alzheimer's disease, Neurobiol. Dis. 46 (2012) 682-691.

[20] J.J. Hoozemans, R. Veerhuis, J.M. Rozemuller, P. Eikelenboom, Neuroinflammation and regeneration in the early stages of Alzheimer's disease pathology, Int. J. Dev. Neurosci. 24 (2006) 157-165.

[21] M. Barad, R. Bourtchouladze, D.G. Winder, H. Golan, E. Kandel, Rolipram, a Type IV-specific phosphodiesterase inhibitor, facilitates the establishment of long-lasting long-term potentiation and improves memory, Proc. Natl. Acad. Sci. U. S. A. 95 (1998) 15020-15025.

[22] V. Lakics, E.H. Karran, F.G. Boess, Quantitative comparison of phosphodiesterase mRNA distribution in human brain and peripheral tissues,

Neuropharmacology 59 (2010) 367-374.

[23] A.S. Sierksma, D.L. van den Hove, F. Pfau, M. Philippens, O. Bruno, E. Fedele, R. Ricciarelli, H.W. Steinbusch, T. Vanmierlo, J. Prickaerts, Improvement of spatial memory function in APPswe/PS1dE9 mice after chronic inhibition of phosphodiesterase type 4D, Neuropharmacology, 77 (2014) 120-130.

[24] S.L. Jin, M. Conti, Induction of the cyclic nucleotide phosphodiesterase PDE4B is essential for LPS-activated TNF-α responses, Proc. Natl. Acad. Sci. U. S. A. 99 (2002) 7628-7633.

[25] C.S. Mclachlan, M.L. Chen, C.N. Lynex, D.L. Goh, S. Brenner, S.K. Tay, Changes in PDE4D isoforms in the hippocampus of a patient with advanced Alzheimer disease, Arch. Neurol. 64 (2007) 456-457.

[26] R. Zebda, A.S. Paller, Phosphodiesterase 4 inhibitors, J. Am. Acad. Dermatol. 78 (2018) S43-S52.

[27] H. Guo, Y. Cheng, C. Wang, J. Wu, Z. Zou, B. Niu, H. Yu, H. Wang, J. Xu, FFPM, a PDE4 inhibitor, reverses learning and memory deficits in APP/PS1 transgenic mice via cAMP/PKA/CREB signaling and anti-inflammatory effects, Neuropharmacology 116 (2017) 260-269.

[28] R. Ricciarelli, C. Brullo, J. Prickaerts, O. Arancio, C. Villa, C. Rebosio, E. Calcagno, M. Balbi, B.T. van Hagen, E.K. Argyrousi, H. Zhang, M.A. Pronzato, O. Bruno, E. Fedele, Memory-enhancing effects of GEBR-32a, a new PDE4D inhibitor holding promise for the treatment of Alzheimer's disease, Sci. Rep. 7 (2017) 46320-46333.

[29] B. Gong, O.V. Vitolo, F. Trinchese, S. Liu, M. Shelanski, O. Arancio, Persistent improvement in synaptic and cognitive functions in an Alzheimer mouse model after rolipram treatment, J. Clin. Invest. 114 (2004) 1624-1634.

[30] Clinical trial study found in clinical trials for roflumilast, NCT01433666 See the following: https://clinicaltrials.gov/ct2/show/NCT01433666?term=NCT01433666&rank=1.

[31] Clinical trial study found in clinical trials for roflumilast,NCT02051335 See the following: https://clinicaltrials.gov/ct2/show/NCT02051335?term=NCT02051335&rank=1.

[32] C. Brullo, R. Ricciarelli, J. Prickaerts, O. Arancio, M. Massa, C. Rotolo, A. Romussi, C. Rebosio, B. Marengo, M.A. Pronzato, B.T.J. van Hagen, N.P. van Goethem, P. D'Ursi, A. Orro, L. Milanesi, S. Guariento, E. Cichero, P. Fossa, E. Fedele, O. Bruno, New insights into selective PDE4D inhibitors: 3-(Cyclopentyloxy)-4-methoxybenzaldehyde O-(2-(2,6-dimethylmorpholino)-2-oxoethyl) oxime (GEBR-7b) structural development and promising activities to restore memory impairment, Eur. J. Med. Chem. 124 (2016) 82-102.

[33] C. Rochais, C. Lecoutey, F. Gaven, P. Giannoni, K. Hamidouche, D. Hedou, E. Dubost, D. Genest, S. Yahiaoui, T. Freret, V. Bouet, F. Dauphin, J. Sopkova de Oliveira Santos, C. Ballandonne, S. Corvaisier, A. Malzert-Fréon, R. Legay, M. Boulouard, S. Claeysen, P. Dallemagne, Novel multitarget-directed ligands (MTDLs) with acetylcholinesterase (AChE) inhibitory and serotonergic subtype 4 receptor

(5-HT4R) agonist activities as potential agents against Alzheimer's disease: the design of donecopride, J. Med. Chem. 58 (2015) 3172-3187.

[34] X. Zha, D. Lamba, L. Zhang, Y. Lou, C. Xu, D. Kang, L. Chen, Y. Xu, L. Zhang, A. De Simone, S. Samez, A. Pesaresi, J. Stojan, M.G. Lopez, J. Egea, V. Andrisano, M. Bartolini, Novel tacrine–benzofuran hybrids as potent multitarget-directed ligands for the treatment of Alzheimer's disease: design, synthesis, biological evaluation, and X-ray crystallography, J. Med. Chem. 59 (2016) 114-131.

[35] X. Li, H. Wang, Y. Xu, W. Liu, Q. Gong, W. Wang, X. Qiu, J. Zhu, F. Mao, H. Zhang, J. Li, Novel vilazodone–tacrine hybrids as potential multitarget-directed ligands for the treatment of Alzheimer's disease accompanied with depression: design, synthesis, and biological evaluation, ACS Chem. Neurosci. 8 (2017) 2708-2721.

[36] M.J. Oset-Gasque, J. Marco-Contelles, Alzheimer's disease, the "one-molecule, one-target" paradigm, and the multitarget directed ligand approach, ACS Chem. Neurosci. 9 (2018) 401-403.

[37] Z. Wang, Y. Wang, W. Li, Z. Liu, Z. Luo, Y. Sun, R. Wu, L. Huang, X. Li, Computer-assisted designed "selenoxy-chinolin": a new catalytic mechanism of the GPx-like cycle and inhibition of metal-free and metal-associated Aβ aggregation, Dalton Trans. 44 (2015) 20913-20925.

[38] B. Wang, Z. Wang, H. Chen, C.J. Lu, X. Li, Synthesis and evaluation of 8-hydroxyquinolin derivatives substituted with (benzo[d][1,2]selenazol-3(2H)-one) as effective inhibitor of metal-induced Aβ aggregation and antioxidant, Bioorg. Med. Chem. 24 (2016) 4741-4749.

[39] Z. Wang, Y. Wang, B. Wang, W. Li, L. Huang, X. Li, Design, Synthesis, and evaluation of orally available clioquinol-moracin M hybrids as multitarget-directed ligands for cognitive improvement in a rat model of neurodegeneration in Alzheimer's disease, J. Med. Chem. 58 (2015) 8616-8637.

[40] D.J. Bonda, X. Wang, G. Perry, A. Nunomura, M. Tabaton, X. Zhu, M.A. Smith, Oxidative stress in Alzheimer disease: A possibility for prevention, Neuropharmacology 59 (2010) 290-294.

[41] L. Di, E.H. Kerns, K. Fan, O.J. McConnell, G.T. Carter, High throughput artificial membrane permeability assay for blood–brain barrier, Eur. J. Med. Chem. 38 (2003) 223-232.

[42] Y. Goriya, C.V. Ramana, The [Cu]-catalyzed SNAR reactions: direct amination of electron deficient aryl halides with sodium azide and the synthesis of arylthioethers under Cu(II)–ascorbate redox system, Tetrahedron, 66 (2010) 7642-7650.

[43] F. Mao, J. Yan, J. Li, X. Jia, H. Miao, Y. Sun, L. Huang, X. Li, New multi-target-directed small molecules against Alzheimer's disease: a combination of resveratrol and clioquinol, Org. Biomol. Chem. 12 (2014) 5936-5944.

[44] K.F. Liew, K.L. Chan, C.Y. Lee, Blood-brain barrier permeable anticholinesterase aurones: synthesis, structure-activity relationship, and drug-like properties, Eur. J. Med. Chem. 94 (2015) 195-210.

[45] G. La Regina, R. Bai, W.M. Rensen, E. Di Cesare, A. Coluccia, F. Piscitelli, V. Famiglini, A. Reggio, M. Nalli, S. Pelliccia, E. Da Pozzo, B. Costa, I. Granata, A. Porta, B. Maresca, A. Soriani, M.L. Iannitto, A. Santoni, J. Li, M. Miranda Cona, F.

Chen, Y. Ni, A. Brancale, G. Dondio, S. Vultaggio, M. Varasi, C. Mercurio, C. Martini, E. Hamel, P. Lavia, E. Novellino, R. Silvestri, Toward highly potent cancer agents by modulating the C-2 group of the arylthioindole class of tubulin polymerization inhibitors, J. Med. Chem. 56 (2013) 123-149.

[46] P. Adlard, R. Cherny, Di, E. Gautier, E. Robb, M. Cortes, I. Volitakis, X. Liu, J. Smith, K. Perez, K. Laughton, Rapid restoration of cognition in Alzheimer's transgenic mice with 8-hydroxy quinoline analogs is associated with decreased interstitial Aβ, Neuron 59 (2008) 43-55.

[47] R.A. Cherny, C.S. Atwood, M.E. Xilinas, D.N. Gray, W.D. Jones, C.A. Mclean, K.J. Barnham, I. Volitakis, F.W. Fraser, Y. Kim, Treatment with a copper-zinc chelator markedly and rapidly inhibits β-amyloid accumulation in Alzheimer's disease transgenic mice, Neuron 30 (2001) 665-676.

[48] J. Hu, Y. Huang, T. Pan, T. Zhang, T. Su, X. Li, H.B. Luo, L. Huang, Design, synthesis, and biological evaluation of dual-target inhibitors of acetylcholinesterase (AChE) and phosphodiesterase 9A (PDE9A) for the treatment of Alzheimer's disease, ACS Chem. Neurosci. (2018) doi: 10.1021/acschemneuro.8b00376.

[49] J.S. Choi, J.J. Braymer, R.P. Nanga, A. Ramamoorthy, M.H. Lim, Design of small molecules that target metal-Aβ species and regulate metal-induced Aβ aggregation and neurotoxicity, Proc. Natl. Acad. Sci. U. S. A. 107 (2010) 21990-21995.

[50] A.C. Souza, M.H. Sari, S. Pinton, C. Luchese, J.S. Neto, C.W. Noqueira, 2-Phenylethynyl-butyltellurium attenuates amyloid-β peptide(25–35)-induced

learning and memory impairments in mice, J. Neurosci. Res. 91 (2013) 848–853.

[51] E. Detrait, T. Maurice, E. Hanon, K. Leclercq, Y. Lamberty, Lack of synaptic vesicle protein SV2B protects against amyloid-β_{25-35}-induced oxidative stress, cholinergic deficit and cognitive impairment in mice, Behavi. Brain Res. 271 (2014) 277-285.

[52] R. Liu, T. Zhang, H. Yang, X. Lan, J. Ying, G. Du, The flavonoid apigenin protects brain neurovascular coupling against amyloid-β_{25-35}-induced toxicity in mice, J. Alzheimers Dis. 24 (2011) 85-100.

Graphical Abstracts

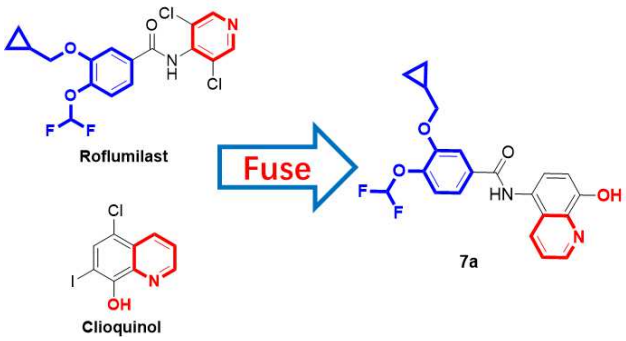

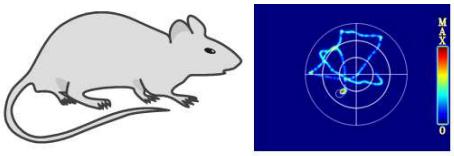

Inhibition of **PDE4D** (IC_{50} = 0.399 μM)

Modulation of metal-induced Aβ aggregation

Intracellular **antioxidant**

Ability of crossing **blood brain barrier** in vitro

Protection of hippocampal neurons from necrosis